SUPPLEMENTAL DATA

METHODS

Reagents

Alexa Fluor 546 (AF546) rat anti-mouse Ly6G mAb (clone 1A8) and Pacific Blue (PB) anti-mouse Ly6G mAb (clone 1A8) were purchased from BioLegend (San Diego, CA). Fluorescein Isothiocyanate (FITC) dextran (MW 70 KDa) and texas-red dextran (MW 70 KDa) were purchased from Molecular Probes Inc. (Eugene, OR). Violet 450 (V450) rat-anti mouse CD49b mAb (clone DX5) was purchased from BD Biosciences (San Jose, CA). GSDMD-NT inhibitor LDC7559[1] was purchased from MedChemExpress (Monmouth Junction, NJ). Pan-caspase inhibitor (Z-VAD-FMK[1]) and GSDMD-NT inhibitor Necrosulfonamide (NSA[2]) were purchased from Millipore Sigma (St. Louis, MO). Caspase-4 inhibitor LEVD-CHO[3] (Cat# 218766) was purchased from EMD Millipore (Taunton, MA). Oxy-Hemoglobin was prepared from lysed human erythrocytes as described elsewhere[4]. Hemin was purchased from Frontier Scientific (Logan, UT). N-Acetyl-L-cysteine (NAC) was purchased from Millipore Sigma. Disulfiram (NSC 190940; Cat# S1680) was purchased from Selleckchem (Houston, TX). Haptoglobin (Product# SRP6507) was purchased from Millipore Sigma. TLR-4 signaling inhibitor (CLI-095; TAK–242) was purchased from InvivoGen. Anti-Neutrophil Elastase Ab (ab21595), rabbit anti-Histone H2A.X mAb (ab124781), and rabbit anti-citrullinated-Histone H3 Ab (ab5103) were purchased from Abcam (Cambridge, MA). Rabbit anti-neutrophil elastase polyclonal antibody, sytox orange, and sytox green were purchased from Thermo Fisher Scientific (Waltham, MA). Ketamine HCl (100 mg/ml) was purchased from Henry Schein Animal Health (Dublin, OH) and xylazine (20 mg/ml) was purchased from LLOYD Laboratories (Shenandoah, IA). Halt™ Protease Inhibitor Cocktail (100X; cat# 78429), RIPA Lysis and Extraction Buffer (cat# 89900), Super Signal Chemiluminescent Substrates WestPico PLUS (cat# 34580), eBioscience™ 1X RBC Lysis Buffer

(cat# 00-4333-57), TBS-Tris Buffered Saline 10X Solution (pH 7.4; cat# BP24711), Sodium Hydroxide Solution N/4 (cat# UN1824), Lab Scientific nonfat dry milk/500G (cat# M0841) and CL-X Posure™ Film (cat# 34091) were purchased from Thermo Fisher Scientific (Waltham, MA). 20X Bolt™ MES SDS Running Buffer (cat# B0002), 20X Bolt™ Transfer Buffer (cat# BT00061), Novex™ Sharp Pre-stained Protein Standard (cat# 21059), 10X Bolt™ Sample Reducing Agent (cat# B0009), nitrocellulose membrane 0.2µm (cat# LC2000) and 4X Bolt™ LDS Sample Buffer (cat# B0008) were purchased from Novex-Invitrogen (Waltham, MA). TWEEN® 20 detergent (CAS 9005-64-5) was purchased from Sigma-Millipore (Burlington, MA). Rabbit anti-mouse β-tubulin Ab (cat# 2146S), rabbit anti-human caspase-4 Ab (cat# 4450S), rabbit anti-human GAPDH Ab (cat# 14C10), rabbit anti-human M-CSF receptor (CD115) Ab (cat# 3152S), HRP-linked horse anti-mouse IgG Ab (cat# 7076), HRP-linked goat anti-rabbit IgG Ab (cat# 7074S) and HRP-linked goat anti-rat IgG Ab (cat# 7077S) were purchased from Cell Signaling (Danvers, MA). Rabbit anti-human-GSDMD Ab (cat# G7422) were purchased from Sigma Aldrich (St. Louis, MO). Rabbit anti-mouse caspase-11 Ab (cat# EPR18628) and rabbit anti-mouse-GSDMD Ab (cat# EPR19828) were purchased from Abcam (Cambridge, MA). FITC-conjugated mouse anti-human CD66b mAb (clone G10F5; cat#561927), APC-conjugated mouse anti-human CD16 mAb (clone 3G8; cat# 561248) and PE-conjugated rat anti-mouse CD11b mAb (clone M1/70; cat# 561689) were purchased from BD Pharmingen (Franklin Lakes, NJ). AF647-conjugated rat anti-mouse Ly6G mAb (clone 1A8; cat# 127609) was purchased from Biolegend (San Diego, CA). Sodium citrate (cat# S1804) was purchased from Sigma Aldrich (St. Louis, MO). Hanks balanced salt solution ($HBSS^-$) without Ca^{2+}, Mg^{2+}, and phenol red formula (cat# 141775095) was purchased from GIBCO (Waltham, MA). MojoSort™ mouse neutrophil negative-selection kit (cat# 480058) and MojoSort™ Magnet (cat# 480019) were purchased from Biolegend (San Diego, CA). RLT+

lysis buffer (cat# 1030963) and RNeasy Plus Micro Kit (cat#74034) were purchased from Qiagen (Hilden, Germany). High-Capacity cDNA reverse transcription kit (cat# 4368814) and PowerUp™ SYBR™ Green Master Mix (cat# A25742) were purchased from Applied Biosystems/Thermo Fischer (Waltham, MA). Ambion™ nuclease-free water (cat# AM9906) was purchased from Life Technologies (Austin, TX). All the primer sequences listed in Supplemental Table 3 were purchased from Integrated DNA Technologies (Coralville, IA). DC™ Protein Assay Kit (Cat#5000111) was purchased from Bio Rad (Hercules, CA). Polymorphprep™ (cat# AXS-1114683) was purchased from Alere Technologies AS (Oslo, Norway). Sterile saline solution (cat# 65207-807-60) was purchased from Nova-Tech (Grand Island, NE). BD Vacutainer 3.2% sodium citrate blood collection 4.5 ml tubes (cat# 369714), 5 ml polystyrene round-bottom tubes (cat# 352058) and BD Precision Glide® needles (cat# 305159) were purchased from BD (Franklin Lakes, NJ). Anti-mouse fibrin Ab (clone 59D8) was a gift from Dr. Rafal Pawlinski at University of North Carolina-Chapel Hill. Gram negative bacterial lipopolysaccharide (LPS) from *Escherichia coli 0111:B4 (E. coli)* was purchased from Sigma-Aldrich (St. Louis, MO).

Mice

Male and female (age ~12-16 weeks old) Townes SCD mice (SS, homozygous for $Hba^{tm1(HBA)Tow}$, homozygous for $Hbb^{tm2(HBG1,HBB*)Tow}$) and non-sickle control mice (AS, homozygous for $Hba^{tm1(HBA)Tow}$, compound heterozygous for $Hbb^{tm2(HBG1,HBB*)Tow}$/$Hbb^{tm3(HBG1,HBB)Tow}$) were used in this study[5]. Townes SS mice have human α and β-sickle (β^S) genes knocked into the locus where mouse α and β genes were knocked out. Townes AS mice are sickle trait mice and thus do not develop SCD. Townes SS and AS mice have been used previously as SCD and control non-sickle mice, respectively[4,6-9]. Townes SS and AS mice were bred and genotyped in-house. P-selectin-

deficient SCD mice (SCD-*Selp*$^{-/-}$) were generated as described elsewhere[10]. Breeding pairs of Gasdermin-D (GSDMD) knock-out (*Gsdmd*$^{-/-}$) mice (Stock# 032410) homozygous for *Gsdmd*^{em4Fcw} allele and the corresponding wild-type (WT) control C57BL/6NJ mice (Stock# 005304) were purchased from Jackson Laboratories (Bar Harbor, ME)[11]. Townes SCD and control mice, SCD-*Selp*$^{-/-}$, and *Gsdmd*$^{-/-}$ mice were bred and genotyped in-house at the University of Pittsburgh, Division of Laboratory Animal Resources (DLAR) facility. All animal experiments were approved by the Institutional Animal Care and Use Committee at the University of Pittsburgh.

Quantitative fluorescence intravital lung microscopy

Quantitative fluorescence intravital lung microscopy (qFILM) has been used widely for *in vivo* assessment of pulmonary vaso-occlusion in SCD mice[4,7,10,12,13]. In the current study, qFILM was used to assess pulmonary vaso-occlusion and detect neutrophil extracellular traps (NETs) in the intact lung microcirculation of live SCD, Control, SCD-*Selp*$^{-/-}$, *Gsdmd*$^{-/-}$ and WT mice following intravenous (IV) challenge with saline, oxy-hemoglobin (oxy-Hb), hemin or LPS with or without pretreatment with GSDMD-NT inhibitors LDC7559[1] or NSA[2] or Disulfiram[14] or the pan-caspase inhibitor Z-VAD-FMK[1] or haptoglobin[9] or TLR4-inhibitor (TAK242)[9]. The qFILM experimental setup and approach has been described elsewhere in detail[12,13]. Briefly, mice were intravenously (IV) administered *via* tail vein with 80 µl of either: 1) saline or vehicle, 2) 10 µmole/kg oxy-Hb, 3) 20 µmole/kg hemin, 4) 0.1 µg/kg LPS[12], 5) 10 µmole/kg oxy-Hb with 10 µmole/kg haptoglobin[9], 6) 0.004 µmol/kg Z-VAD-FMK or 10 mg/kg LDC7559 or 20 mg/kg NSA or 10 mg/kg Disulfiram or 10 mg/kg TAK242[9], 30 min prior to 10 µmole/kg oxy-Hb. Approximately 2-

2.5 hours following IV administration, qFILM was conducted with a Nikon multi-photon-excitation fluorescence microscope using an excitation wavelength of 850 nm and an APO LWD 25x water immersion objective with 1.1 NA. Time-series of 2D qFILM images were collected at ~15 frames per second (fps) using a resonant scanner. Each field of view (FOV) was 256 μm x 256 μm (~65,536 μm^2) with a resolution of ~0.5 μm per pixel in the x-y plane. Fluorescent light received from the sample was collected in several band pass filters including 450/20 nm (detector 1 for collection of V450 or Pacific Blue), 525/50 nm (detector 2 for collection of FITC), 576/26 nm (detector 3 for collection of AF546), and 685/70 nm (detector 4 for collection of Evans Blue). Before imaging, mice were anesthetized with an intraperitoneal (IP) injection of 100 mg/kg ketamine HCl and 20 mg/kg xylazine. A cannula was inserted into the right carotid artery and a tracheotomy was performed to facilitate mechanical ventilation with 95% O_2 and supply maintenance anesthesia (1-2% isoflurane). The left lung was surgically exposed, and a small portion of the lung was immobilized against a coverslip using a vacuum enabled micro-machined device as described elsewhere[13,15]. Just prior to qFILM, ~125 μg/mouse FITC-dextran or 50 μl Evans Blue, 5 μg/mouse Sytox Orange or Green, 10 μg/mouse AF546-conjugated anti-NE Ab, 10 μg/mouse AF546-conjugated anti-citrullinated-histone-3 (H3cit) Ab, 12 μg/mouse AF546 or Pacific Blue-conjugated anti-Ly6G mAb and 7 μg/mouse V450-conjugated anti-mouse CD49b mAb were injected into the carotid artery catheter for visualization of the pulmonary microcirculation, extracellular DNA and *in vivo* staining of NE, citrullinated-histones, neutrophils and platelets, respectively. These fluorescent Abs and dyes have been used widely in the past for visualization of neutrophils, platelets and NETs in intravital microscopy studies[7,10,12,13,15-22]. QFILM was performed on a mouse for a total period of 30 minutes and the presence or absence of vaso-occlusion, presence or absence of NETs, and counts of circulating NETs (cNETs) were

assessed for 30 seconds in each FOV. The resulting series of qFILM images were processed using image subtraction, a median filter, a noise-reduction algorithm, and adjustment of intensity histograms as described previously[4,7,10,12]. As described in the figure legends, some of the channels were pseudo-colored to enhance contrast. Pulmonary vaso-occlusions were assessed in ~10-15 FOVs in each mouse and across multiple mice per test group (n = 3 to 6) as previously described[4,7,10,12].

QFILM image processing and data analysis

Time series of qFILM 2D-images were processed and analyzed using Nikon's NIS-Elements software (Nikon Instruments; Tokyo, Japan) as described elsewhere[7,12]. First, image subtraction was performed to remove autofluorescence between channels. Second, signal to noise ratio was improved by using median filter, smoothing and denoising functions. Third, each channel was pseudo-colored as following: microcirculation as violet, neutrophils primarily as red or blue in some instances, platelets as green, extracellular DNA as green, NE as red and histones as red. Pulmonary vaso-occlusions were defined using the following criteria described previously[4,7,12]. Briefly, a pulmonary vaso-occlusion was defined as a neutrophil-platelet aggregate (> 500 μm^2 in size) occluding a pulmonary arteriole (> 20 μm ID) or the arteriolar bottle-neck (junction between a pulmonary arteriole and the downstream pulmonary capillaries), leading to impairment of arteriolar blood flow. Pulmonary vaso-occlusions were quantified and compared between treatment groups using the following four parameters as described previously[4,7,12]: 1) Average number of pulmonary vaso-occlusions per FOV, 2) Percent FOVs with at least one pulmonary vaso-occlusion, 3) Average number of large pulmonary vaso-occlusions (size > 1000 μm^2) per FOV, and 4) Average number of neutrophil-rich (primarily composed of neutrophils with few

platelets) or platelet-rich (primarily composed of platelets with few neutrophils) pulmonary vaso-occlusions per FOV. Based on previous studies[17,19,21], a NET in the qFILM image was identified using one of the following criteria: 1) a strand of extracellular DNA colocalizing with NE or citrullinated-histones (H3cit); 2) a strand of extracellular DNA either colocalizing or within ~ 5 μm proximity of one or more neutrophil (Ly6g-staining). Number of NETs were counted in each FOV, and average number of NETs per FOV compared between treatment groups. Circulating NETs (cNETs) were identified as fragments of extracellular DNA flowing into the lung through the pulmonary arteriole. NIS-Elements software was used to quantify the number of cNETs entering each FOV over a 30 seconds duration, to estimate average number of cNETs entering per FOV per minute (#cNETs/FOV/min), which was compared between treatment groups.

Quantitative Liver Intravital Microscopy

Recently, we developed quantitative liver intravital microscopy to study liver pathophysiology in SCD mice[6,23]. In the current study, liver intravital microscopy was used to detect NETs generation in the intact liver microcirculation of live mice. Liver intravital microscopy was conducted on same strains of mice as described under qFILM studies. The liver intravital microscopy experimental setup has been described previously in detail[6,23,24]. Briefly, mice were IV administered *via* tail vein with 80 μl of either: 1) saline, 2) 10 μmole/kg oxy-Hb, 3) LDC7559 (10 mg/kg) or TAK242 (10 mg/kg), 30 min prior to 10 μmole/kg oxy-Hb. Mice were anesthetized with an IP injection of 100 mg/kg of body weight ketamine HCl and 20 mg/kg of body weight xylazine. Following anesthetization, mice were IP administered 1 ml physiological saline (maintained at room-temperature) and placed on a heated stage in the supine position. Next, the right carotid artery was cannulated with heparinized PE10 tubing. Mice were repositioned in the supine

position, the right lobe of the liver was exposed and gently immobilized against a coverslip using a vacuum-enabled micro-machined liver-imaging window described elsewhere[6,23-25]. Next, ~125 μg/mouse FITC/Texas-red-dextran, 5 μg/mouse Sytox Orange/Green, and 12 μg/mouse AF546 or Pacific Blue-conjugated anti-Ly6G mAb were injected into the carotid artery catheter for visualization of the liver microcirculation, extracellular DNA, and *in vivo* staining of neutrophils, respectively, and intravital observations were conducted in the intact mice liver with a Nikon multi-photon-excitation fluorescence microscope using an excitation wavelength of 850 nm and an APO LWD 25x water immersion objective (1.1 NA) as described elsewhere in detail[6,23-25]. Time series of intravital 2D-images were processed and analyzed using Nikon's NIS-Elements software, each channel was pseudo-colored (microcirculation as violet, neutrophils as red, and extracellular DNA as green) and NETs in the liver were quantified using the same strategy as the one used for qFILM image processing. Average number of NETs per FOV (~65,536 μm^2) was quantified and compared between treatment groups.

Strategy to halt the blood flow from the liver to the lung in mice

As shown in the Supplemental Figure 12, blood enters the liver through the hepatic artery and portal vein, travels through the liver sinusoids, and then exits through the multiple short branches of hepatic vein that drain into the Inferior-Vena-Cava (IVC). IVC carries blood to the right-heart and lung. In mice, the hepatic vein branches are short in length, primarily embedded inside the liver tissue and drain individually into IVC, thus making it hard to clamp all of them simultaneously without causing trauma. Therefore, the blood flow through the liver to lung was stopped by simultaneously clamping the hepatic artery and portal vein (Supplemental Figure 12) using a silk suture ligature, which was confirmed using liver intravital microscopy (Video 17).

Video 17 shows the presence and absence of blood flow through the liver pre and post ligature, respectively of the portal vein and hepatic artery. For studies described in Figure 3H-I and Supplemental Figure 13, the arrival of cNETs in the lung was confirmed using qFILM, then the hepatic artery and portal vein were simultaneously clamped (using a ligature) to stop the blood outflow from the liver into the IVC, and the effect on cNETs arrival in the lung was again assessed using qFILM in the same mice.

Quantitative Kidney Intravital Microscopy

Intravital microscopy was conducted for *in vivo* visualization of blood flow, blood cell trafficking and detection of NETs in the intact kidney of live SCD mice, using an experimental set-up and approach identical to the one used for liver intravital microscopy. Briefly, mice were IV injected *via* tail vein with 10 μmole/kg oxy-Hb, anesthetized, and prepared for intravital imaging. Mice were positioned in the supine position, the right kidney was exposed and gently immobilized against the cover slip using a vacuum-enabled micro-machined imaging window. Next, intravascular fluorescent dyes and Abs similar to the one used in liver intravital microscopy were IV administered through the carotid artery catheter for visualization of the kidney microcirculation, extracellular DNA, and *in vivo* staining of neutrophils, and intravital observations in the intact mice kidney were conducted using the Nikon-multiphoton excitation fluorescence microscope set-up similar to the one used in liver intravital microscopy. Time series of intravital 2D-images were processed and analyzed using a strategy similar to the one used for liver intravital microscopy.

Confocal microscopy of fresh liver slices

The method of liver confocal imaging is described elsewhere[24]. Briefly, SCD and control mice were IV administered 10 μmole/kg oxy-Hb, sacrificed 3 hours later and livers harvested. Freshly harvested (unfixed) liver tissue was sectioned into ~50 μm slices. Liver slices were attached to glass slides, incubated with Pacific Blue-anti-Ly6G Ab, sytox green and AF546-anti-neutrophil elastase (NE) Ab to stain neutrophils, extracellular DNA and NE, respectively, and images were captured using an inverted Nikon laser-scanning confocal microscope. NETs were identified as triple-positive for NE (red), extracellular DNA (green), and neutrophil marker Ly6G (pseudo-colored white for better visualization) using the strategy described elsewhere[21]. Confocal images were processed and analyzed using Nikon's NIS-Elements software. NETs were counted in several FOVs (FOV size ~166,547 μm^2) and average number of NETs per FOV (#NETs/FOV) was compared between groups.

Blood collection from human subjects

Healthy race-matched control human subjects (control) and steady state (not in crisis) SCD (SS or S/β^o) patient blood was collected via venipuncture in a blue-cap glass BD Vacutainer tube containing sodium citrate (BD Biosciences, Franklin Lakes, NJ) in accordance with the guidelines set by the Institutional Review Board at the University of Pittsburgh. The procedure for blood draw has been described elsewhere in detail[7,12]. Only non-smokers who were not on chronic transfusion therapy (no transfusion within the last 1 month) were included in the study. Informed written consent was obtained from all the participants in accordance with the Declaration of Helsinki. All blood samples were used within 2 hours of blood draw.

Imaging flow cytometry of SCD patient plasma

SCD patient blood was split into following treatment groups: 1) untreated or incubated for 15 min with 2) 20 μM hemin, 3) 20 μM hemin + 20 μM LDC7559, 4) 20 μM hemin + 20 μM caspase-4 inhibitor (LEVD-CHO), and 5) 20 μM hemin + 20 μM NAC. Following incubation, blood samples were processed to generate platelet-poor-plasma (PPP) as described elsewhere[7]. For each treatment group, 30 μl of PPP was mixed with 70 ul of physiological saline, and incubated with sytox green, AF546-conjugated anti-NE Ab, and AF647-conjugated-anti-H3cit or H2A.X Ab for *in situ* staining of extracellular DNA, NE, and histones, respectively. Imaging flow cytometry was conducted using Image Stream equipment (Amnis, Seattle, WA) and data was analyzed using IDEAS application software version 6.2.187.0 (Amnis). cNETs were identified as particles (< 3 μm) triple-positive for NETs markers-extracellular DNA, NE and histones. As shown by the representative images in Figure 2K, Channel 1 showed the bright field image, channel 2 showed extracellular DNA (green), channel 3 showed histones (yellow) and channel 4 showed NE (red). Concentration of cNETs was reported as number of cNETs per μl of plasma and compared between treatment groups.

Imaging flow cytometry of SCD mice plasma

SCD or SCD-*Selp-/-* mice were IV administered 10 μmole/kg Oxy-Hb ± 10 mg/kg LDC7559. After 3 hours, mice were sacrificed, blood was drawn *via* inferior vena cava into tubes containing 3.2% sodium citrate (0.105M) in a ratio of 1:10 (sodium citrate : blood), and processed to generate platelet-poor-plasma (PPP) as described elsewhere[7]. Samples were stained and cNETs were detected by imaging flow cytometry using the same approach used for SCD patient plasma.

Representative images shown in Figure 2H. Concentration of cNETs was reported as number of cNETs per µl of plasma and compared between treatment groups.

Isolation of neutrophils from murine blood

MojoSort™ mouse neutrophil negative-selection kit (Biolegend, San Diego CA) was used to isolate neutrophils from murine blood using the protocol described elsewhere[26]. SCD or control mice blood (0.75ml) was drawn into 3.2% sodium citrate as an anticoagulant (ratio of 1:10) from inferior-vena-cava using a 22g needle (BD), mixed with 6 ml of $HBSS^-$ (without Ca^{2+} or Mg^{2+}) in a 15 ml conical-bottom BD falcon tube, and centrifuged at 300g for 5 min at room temperature. The cell pellet was resuspended in 500 µl of MojoSort™ buffer (provided with MojoSort™ kit) at a concentration of ~$1x10^8$ cells/ml, the resulting cell suspension was transferred into 5 ml round bottom tube (BD) and 50 µl biotin-antibody cocktail (provided with MojoSort™ kit) was added. The solution was gently mixed and incubated at room temperature for 15 minutes. Up to 4 ml MojoSort Buffer was added to wash the cells, followed by centrifugation at 300g for 5 minutes. The supernatant was discarded and the pellet was resuspended in 500 µl of MojoSort buffer. Streptavidin-coated magnetic nanobeads (provided with MojoSort™ kit) were briefly vortexed, 50 µl of beads were added to the cell suspension, and incubated at room temperature for 15 minutes. After 15 minutes, up to 4ml of MojoSort buffer was added to the tube containing mixture of beads and cells, and the tube was centrifuged at 300g for 5 minutes. The supernatant was discarded, the pellet was resuspended in 2 ml of MojoSort buffer, and the tube was placed in the MojoSort Magnet for 5 minutes. Cells labeled by the complex of biotin-Ab cocktail and streptavidin-magnetic nanobeads were retained in the tube, while supernatant containing unlabeled cells (neutrophils) was gently transferred into a second collection tube. Flow cytometry was used

to confirm neutrophil purity (>98%) based on percent Ly6G+ cells (Supplemental Figure 14) as described elsewhere[12,27,28].

Isolation of neutrophils from human blood

Venous blood (~4.5 ml each tube) was drawn from SCD or control human subjects into 3.2% sodium citrate BD Vacutainers (BD) and incubated for 15 min with either 1) saline as a vehicle, 2) 20 μM hemin, 4) 20 μM hemin + 20 μM caspase-4 inhibitor LEVD-CHO, and 4) 20 μM hemin + 20 μM NAC. After the incubation, blood was transferred into a 15 ml BD Falcon tube containing 4.5 ml of PolymorphPrep®, and centrifuged at 450g for 30 minutes at room temperature (22°C) with minimal acceleration and no brakes as described elsewhere[29]. After centrifugation, the neutrophil-containing layer was carefully pipetted into a new 15 ml falcon tube as per the vendors' instructions, diluted with $HBSS^-$ (without Ca^{2+} or Mg^{2+}) to a total volume of 10 ml, and then centrifuged at room temperature for 8 minutes at 450g. The resulting pellet containing neutrophils and residual erythrocytes was resuspended in 2 ml of erythrocyte (RBC) lysis buffer (Thermo Fisher Scientific) for 20 seconds, followed by dilution with HBSS (without Ca^{2+} and Mg^{2+}) to a total volume of 10 ml and centrifugation at room temperature for 8 minutes at 450g. The last step was repeated 2-3 times until no erythrocytes were visible in the pellet. Finally, the neutrophil-rich pellet was used in western blotting studies. Neutrophil purity was determined by using two approaches. In first approach (Supplemental Figure 17A), the percentage of neutrophils was confirmed to be greater than 95% using flow cytometry by identifying neutrophils as cells dual positive for CD16 and CD66b as described previously[30]. In second approach (Supplemental Figure 17B), western blotting was used to confirm absence of any contamination by monocytes based on absence of monocyte marker CD115.

Western blotting of human and murine neutrophils

Isolated neutrophils were resuspended in 200 µl RIPA lysis buffer (50 mmol/L Tris-403 HCl, pH 8.0; 150 mmol/L NaCl; 1% NP-40; 0.5% sodium deoxycholate; 0.1% sodium dodecyl sulfate; ThermoFisher Scientific) maintained at 4°C and enriched with HALT® Protease & Phosphatase Inhibitor Cocktail (Thermo Scientific) in a ratio of 1:100. Lysates were centrifuged at 15,000g for 12 minutes and protein concentration was measured using colorimetric Detergent Compatible Bio-Rad assay (Bio-Rad). The total protein (50 µg per sample) was reduced using Bolt®/NuPage® Reducing Agent (Novex) for 2 minutes at 85°C, and subsequently separated on Bolt® Mini-Gel (Invitrogen) using 5% MES SDS Running Buffer (Novex) for 27-40 minutes (depending on the molecular weight of the analyzed protein) using 200V and 500mA power settings. Afterwards, proteins were electro-transferred onto 0.2 µm pore-size nitrocellulose membrane (Novex) using 10 V and 500 mA power settings for 60 minutes. Membranes were blocked using 5% non-fat milk in Tris-buffered saline (ThermoFisher), supplemented with 0.05% Tween-20 (TBS-T) for 45 minutes at room temperature, and then rinsed 3x for 10 minutes with TBS-T, followed by an overnight incubation with diluted primary antibodies (1:500-1:1000) in TBS-T containing 5% of non-fat milk at 4°C (Supplemental Table 1 shows the list of primary Abs and the dilutions used). After the overnight incubation, membranes were washed 3x for 10 minutes with TBS-T at room temperature and incubated for 1 hour at room temperature with the secondary antibodies diluted in TBS-T with 5% non-fat milk (1:2000-1:10000; refer to Supplemental Table 2 for the list of secondary Abs and the dilutions used). Membranes were rinsed 3x for 10 minutes with TBS-T and treated with SuperSignal® Chemiluminescent Substrate (ThermoFisher) for 2 minutes in the dark. Films were developed using Konica SRX-101A, and analyzed using NIH-ImageJ software. Next, immunoblots were washed with TBS-T, immersed in stripping buffer (Thermo Fisher Scientific)

for 20 minutes, membranes washed with TBS-T, blocked with non-fat milk for 45 minutes, and then used for immunoblotting with primary Abs against house-keeping controls GAPDH (human) or β-tubulin (murine) followed by respective secondary Abs.

mRNA analysis of murine neutrophils

Murine neutrophils were isolated from whole blood as described in the previous section, and immediately transferred into the tube containing RLT plus lysis buffer (Qiagen) enriched with 1% β-mercaptoethanol (Sigma Aldrich). In each sample, total RNA was extracted from murine neutrophils by using RNeasy Plus Micro Kit (Qiagen). After confirming RNA integrity using NanoDrop 8000 Spectrophotometer (Thermo-Fisher), 2 μg of total RNA was used as a template to prepare first-strand complementary DNA (cDNA) using a high capacity cDNA reverse transcription kit (Applied Biosystems). Quantitative-reverse-transcription-polymerase chain reaction (qRT-PCR) analyses were performed using an Applied Biosystems StepOnePlus™ Real-Time PCR System (Applied Biosystems, Foster City, CA) with PowerUp™ SYBR™ Green Master Mix (Applied Biosystems/Thermo Fischer, Waltham, MA) in a 60-cycle PCR. Initial denaturation of DNA template was conducted at 95°C for 10 minutes. The denaturing, annealing and extension conditions of each PCR cycle were 95°C for 10 min, 60°C for 58 s and 95°C for 15 s, respectively. As described elsewhere[31], *Rack1* was selected as the house-keeping gene for mRNA-analyses in neutrophils. The relative amount or fold-change of the target gene expression was normalized relative to the level of *Rack1* (house-keeping) gene and relative to control mice[31]. Mathematical model of log2 fold change (relative expression) was used to normalize the data as described elsewhere[32]. The primer sequences used in the qRT-PCR are listed in Supplemental Table 3.

Statistical analysis

The average number of pulmonary vaso-occlusions per FOV, the average number of pulmonary vaso-occlusions (per FOV) with area > 1000 μm^2, average number of NETs per FOV, average number of cNETs per FOV per minute, and average number of cNETs per µl of plasma were compared between groups using the unpaired Student's *t* test with Bonferroni correction or one-way ANOVA with Games-Howell's multiple comparisons test when comparing more than two groups. The percent FOVs with pulmonary vaso-occlusions were compared between groups using the four-fold table analysis with $\chi 2$ statistics as described elsewhere[4,7,12]. Error bars represent mean ± standard error (SE). A *p* value less than 0.05 was considered as significant. In western blot analyses, the measured intensity of the bands were normalized to the corresponding loading control (GAPDH for human, β-tubulin for murine). Unpaired or paired two-tailed Student's *t*-test were used to confirm the significance. The mean Log2 fold-change in mRNA analyses were compared using the Student *t*-test. The levels of statistical significance were as follows: $*p < 0.05$; $**p < 0.01$. The heatmap for the genes expression was drawn using GraphPad 7 Prism software.

SUPPLEMENTARY TABLES

Supplemental Table 1. The list of primary Abs used in western blot studies.

Primary Ab	Manufacturer	Catalog No.	Dilution
Rabbit anti-β-tubulin	Cell Signaling	2146S	1:500
Rabbit anti-Caspase-4	Cell Signaling	4450S	1:500-1:1000
Rabbit anti-Caspase-11	Abcam	EPR18628	1:500
Rabbit anti-GAPDH	Cell Signaling	14C10	1:1000-1:2000
Rabbit anti-human GSDMD	Sigma Aldrich	G7422	1:1000
Rabbit anti-mouse GSDMD	Abcam	EPR19828	1:500
Rabbit anti-mouse CD115	Cell Signaling	3152S	1:1000

Supplemental Table 2. The list of secondary Abs used in western blot studies.

Secondary Ab	Manufacturer	Catalog No.	Dilution
Anti-Mouse IgG; HRP-linked	Cell Signaling	7076	1:10000
Anti-Rabbit IgG; HRP-linked	Cell Signaling	7074S	1:2000-1:10000
Anti-Rat IgG; HRP-linked	Cell Signaling	7077S	1:10000

Supplemental Table 3. The list of primers used in mRNA analyses.

Gene	Forward primer	Reverse primer
Gsdmd	CCA TCG GCC TTT GAG AAA GTG	ACA CAT GAA TAA CGG GGT TTC C
Casp11	CAG ACA TCA GAC AGC ACA TTC	AGC AGC GTG GGA GTT C
Mpo	TCC CAC TCA GCA AGG TCT T	TAA GAG CAG GCA AAT CCA G
Elane	GTT GGG CAC AAA CAG ACC	GCA AAC TCA GCC ACA GG
Pad4	CGA TTG GCT CTT TGT GGG TC	CCG AAA ACC CTG CTT GTC C
Tyk2	TTG GGA TCT AGA TCC TGC CTC AGC TTC CCA CGT	GGT ACG GTC GAC TTC CTT CCT GTC CGC AGC CAG
Stat1	AGG GGC CAT CAC ATT CAC AT	AGA TAC TTC AGG GGA TTC TC
Jak1	CTT TCG GTG CCT CTC CTT AG	AGA GCT GAT CAC TTC CGT GT
Jak2	CAA ACT AAA GAA GGC GGG TA	TGA CAT TTT CTC GCT CAA CA
Irf1	CAG AGG AAA GAG AGA AAG TCC	CAC ACG GTG ACA GTG CTG G
Irf2	GGA CTC AGC AGC TCT ACC CTA	CAG TTG AGT CAT CTT TGG GGC
Irf7	CCT CTG CTT TCT AGT GAT GCC G	CGT AAA CAC GGT CTT GCT CCT G
Irf9	CAA CAT AGG CGG TGG TGG CAA T	GTT GAT GCT CCA GGA ACA CTG G
Ticam1	CAG CTC AAG ACC CCT ACA GC	CTC CCA CAC AGC CTC GTC
Ifnar1	AGC CAC GGA GAG TCA ATG G	GCT CTG ACA CGA AAC TGT GTT TT
Casp1	TTG GAG CTC AAG TTG ACC TC	TTC CCT CCT GGA TAC CAT GA
Gsdme	AGC TCT TTG CAA CAG CCT ACT TCC	TGT GGC ATT ATC AGG CAT TTC TGC
Cxcr2	GGC GGG GTA AGA CAA GAA TC	GGC AAG GTC AGG GCA AAG AA
Cxcr4	TCA GTG GCT GAC CTC CTC TT	CTT GGC CTT TGA CTG TTG GT

Ifna	TCA AAG GAC TCA TCT GCT GCT TG	CCA CCT GCT GCA TCA GAC AAC
Ifnb1	CAG CTC CAA GAA AGG ACG AAC	GGC AGT GTA ACT CTT CTG CAT
Ifng	TGC TGA TGG GAG GAG ATG TCT AC	ACC TGA CAC ATT CGA GTG CTG T
Itgam	AAA CCA CAG TCC CGC AGA GA	CGT GTT CAC CAG CTG GCT TA
Rack1	GAG TGT GGC CTT CTC CTC TG	GCT TGC AGT TAG CCA GGT TC

SUPPLEMENTAL FIGURES

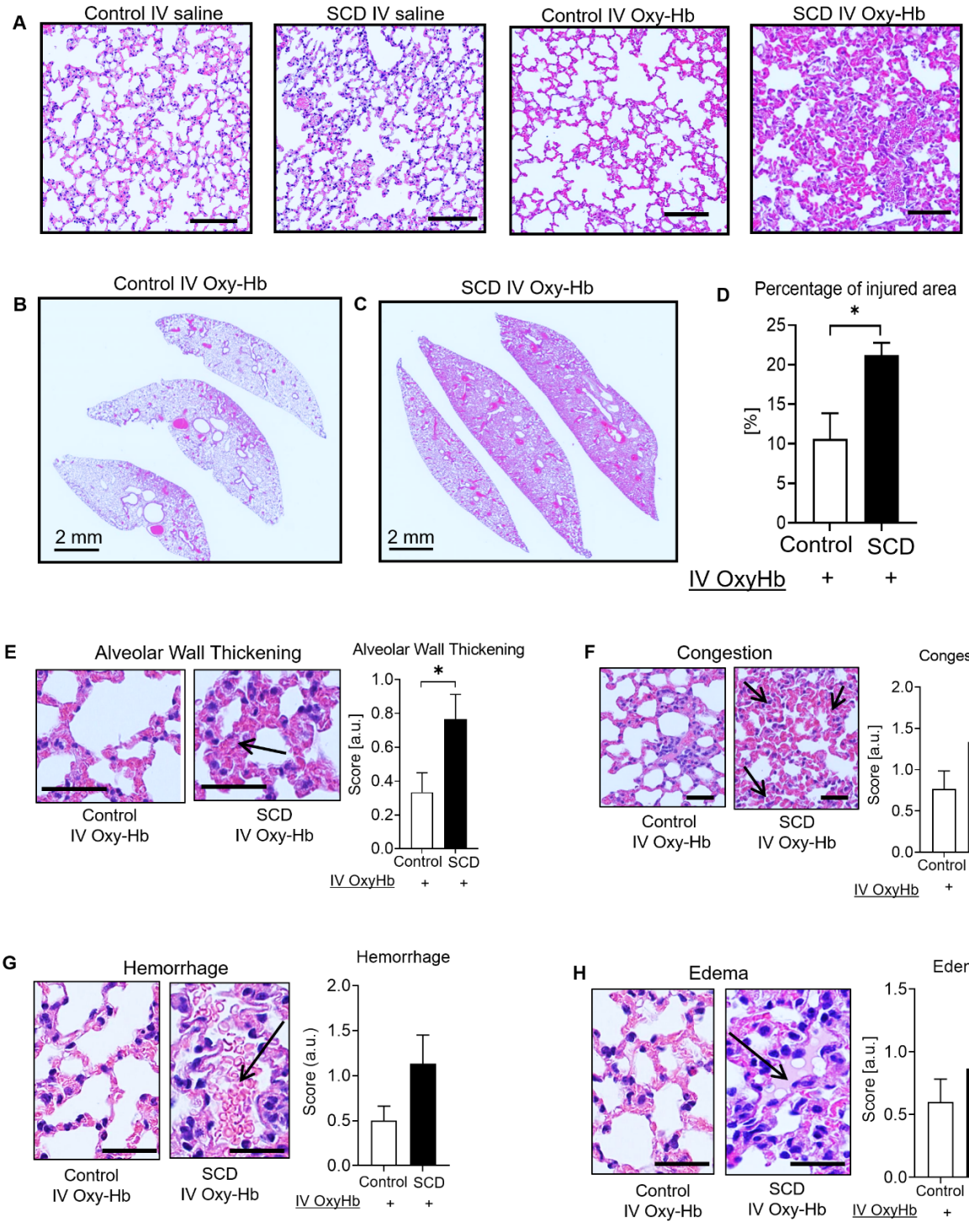

Supplemental Figure 1. Intravenous challenge with oxy-hemoglobin promotes lung injury in SCD mice. (A) Hematoxylin and eosin (H&E) stained lung histology of control and SCD mice, 3

hours post intravenous (IV) administration of saline or 10 μmole/kg oxy-hemoglobin (oxy-Hb). H&E stained three representative whole lung slices of a **(B)** control mouse and **(C)** SCD mouse intravenously (IV) administered 10 μmole/kg oxy-Hb. **(D-H)** Lung histology was scored to assess lung injury using American Thoracic Society guidelines. **(D)** Percent injured area and **(E)** alveolar wall thickening were significantly higher in SCD than control mice administered IV oxy-Hb. Although **(F)** congestion, **(G)** hemorrhage, and **(H)** edema also seemed higher in SCD than control mice administered IV oxy-Hb, these differences did not reach significance. Representative images in E-H show difference in pathology between control and SCD mice administered IV oxy-Hb. n = 5 mice per group. Data represents Mean ± SE. Means compared using unpaired students *t*-test. * $p < 0.05$. Scale bars 200 μm (A), 2 mm (B-C) and 20 μm (E-H).

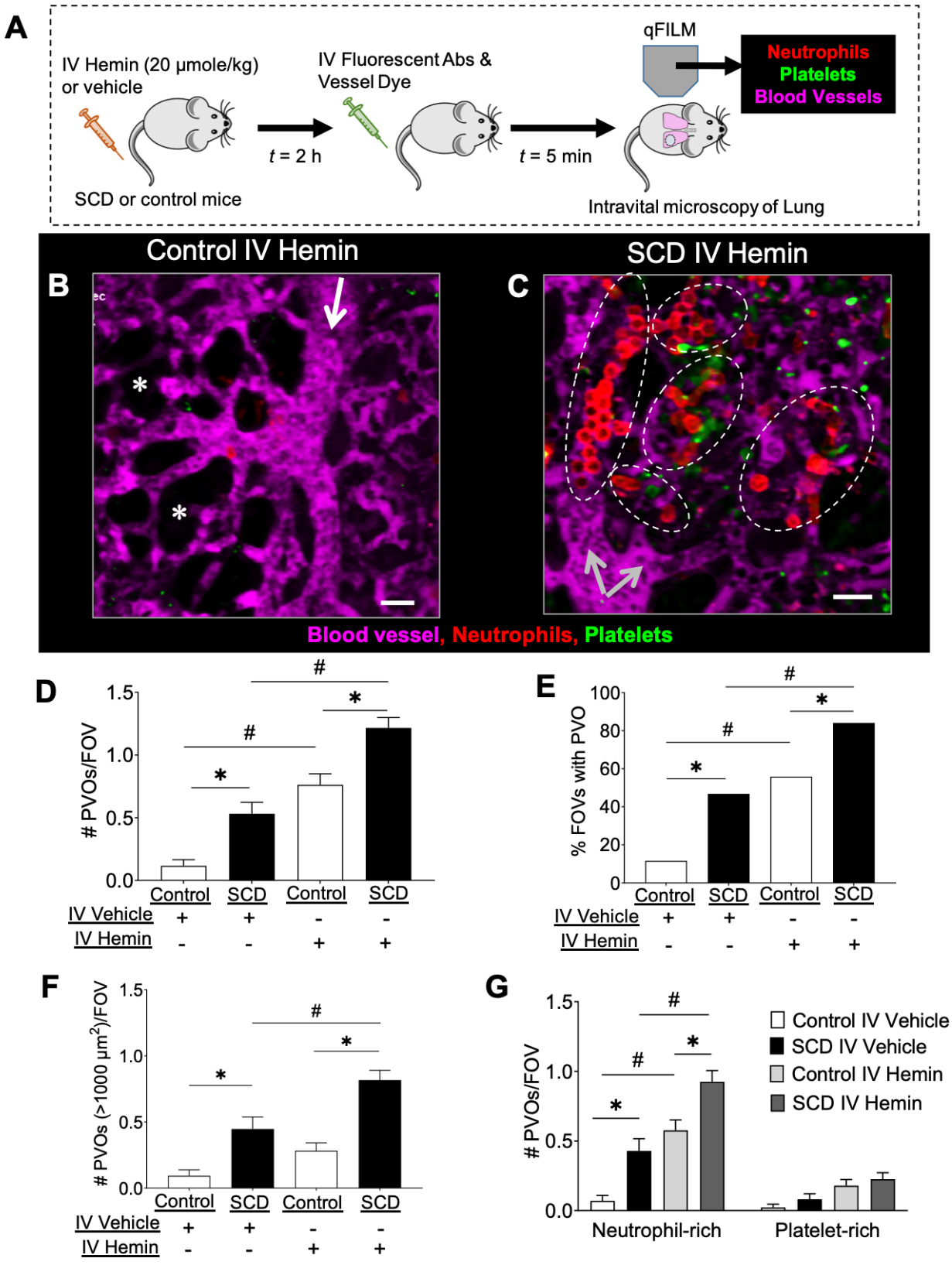

Supplemental Figure 2. Intravenous challenge with hemin promotes lung vaso-occlusion in

SCD mice. (A) Experimental scheme: Control and SCD mice were IV administered 20 μmole/kg hemin or saline (vehicle), and quantitative fluorescence intravital lung microscopy (qFILM) was used to assess the absence or presence of platelet-neutrophil aggregate mediated pulmonary vaso-occlusion. Pulmonary microcirculation (pseudo-colored purple), neutrophils (red) and platelets (pseudo-colored green) were labeled *in vivo* by IV administration of FITC dextran, AF546-anti-Ly6G Ab and V450-anti-CD49b Ab, respectively. Representative qFILM images are shown in B-C. **(B)** IV hemin led to minimal lung vaso-occlusion in a control mouse. Video 3 shows circulating neutrophils (red) and erythrocytes (dark cells) transiting through the pulmonary arteriole and into the pulmonary capillary bed, suggestive of unobstructed pulmonary blood flow. **(C)** IV hemin led to occlusion of arteriolar bottle-necks in the lung of an SCD mouse by large neutrophil-platelet aggregates (marked by dotted white ellipses). In Video 4, cells upstream of aggregates in the main arteriole move back and forth, suggestive of an obstructed blood flow. White arrows denote the direction of blood flow within the pulmonary arterioles. Alveoli are marked with asterisks. Scale bars 20 μm. Diameter of pulmonary arteriole in B and C is 32.6 and 29.5 μm, respectively. **(D-G)** Pulmonary vaso-occlusions (PVOs) were quantified using strategy described in Supplemental Methods. IV hemin led to significantly more **(D)** PVOs per FOV, **(E)** percent FOVs with PVOs, **(F)** large PVOs (with area > 1000 μm^2) per FOV, and **(G)** neutrophil-rich PVOs per FOV, in SCD compared to control mice. Control IV vehicle (n=3 mice; 43 FOVs), SCD IV vehicle (n=3 mice; 44 FOVs), control IV hemin (n=5 mice; 77 FOVs), SCD IV hemin (n=5 mice; 88 FOVs). qFILM FOV size~65,536 μm^2. * denotes $p < 0.05$ for SCD compared to control. # denotes $p < 0.05$ for IV hemin compared to IV vehicle. Data in D, F and G represent Mean ± SE and compared using *t*-test with Bonferroni correction. Percentages in E compared using 4-fold table analyses with Bonferroni χ^2 statistics.

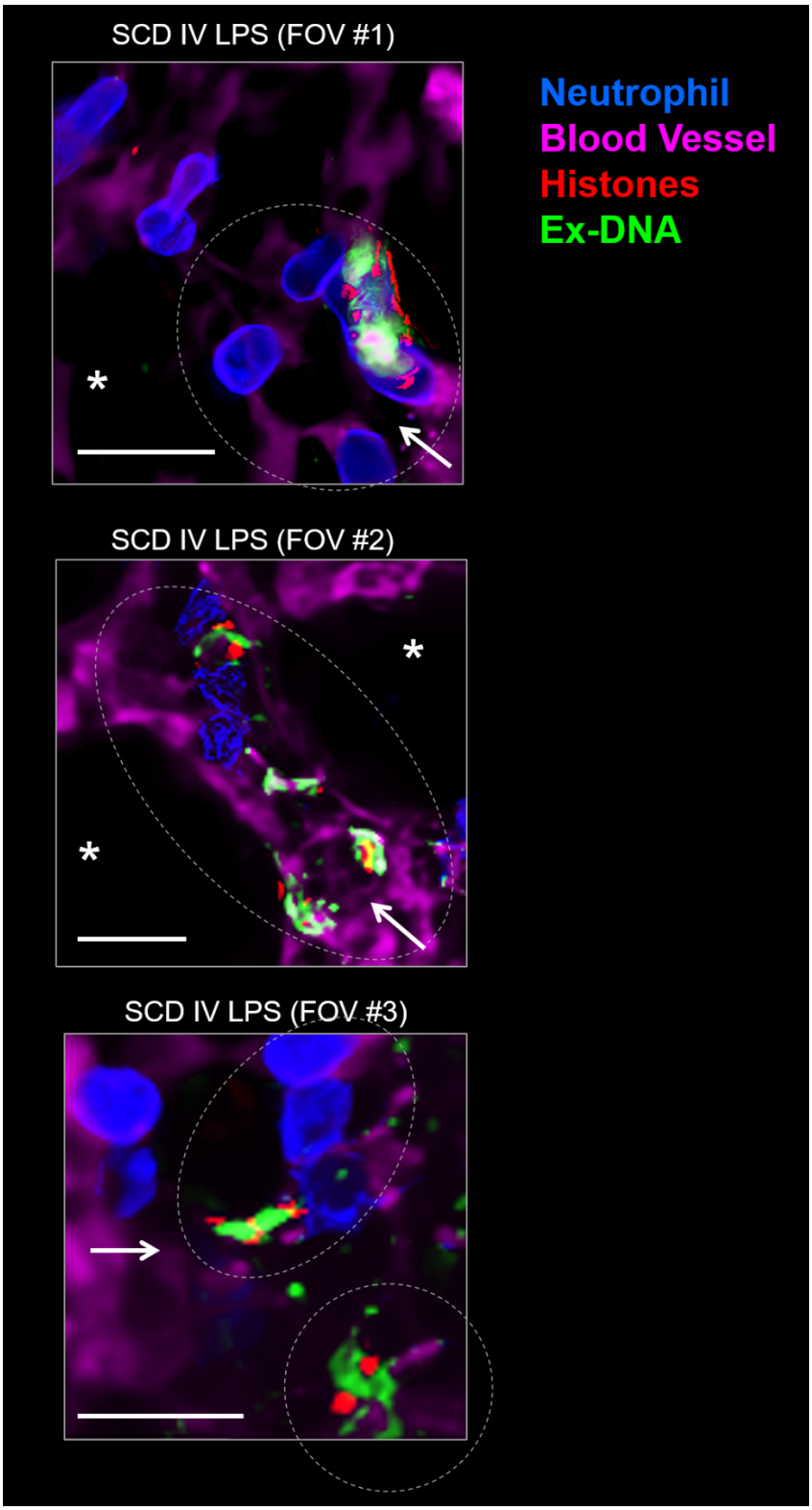

Supplemental Figure 3. NETs promote lung vaso-occlusion in SCD mice *in vivo*. SCD mice

were IV administered 0.1 μg/kg LPS and quantitative fluorescence intravital lung microscopy (qFILM) was used to assess the absence or presence of NETs within the pulmonary microcirculation. Pulmonary microcirculation (pseudo-colored purple), neutrophils (blue), extracellular DNA (green), and histones (red) were labeled *in vivo* by IV administration of Evans Blue, Pacific Blue-anti-Ly6G Ab, Sytox Green and AF546-anti-Histone H2A.X Ab, respectively. Three representative qFILM images reveal NETs (marked by dotted white ellipse) in the pulmonary arteriole bottle-necks of SCD mice administered IV LPS. NETs were identified based on colocalization of Ly6G (blue) with exDNA (green) and histones (red). White arrows denote the direction of blood flow. Alveoli are marked with white asterisks. Scale bars 20 μm.

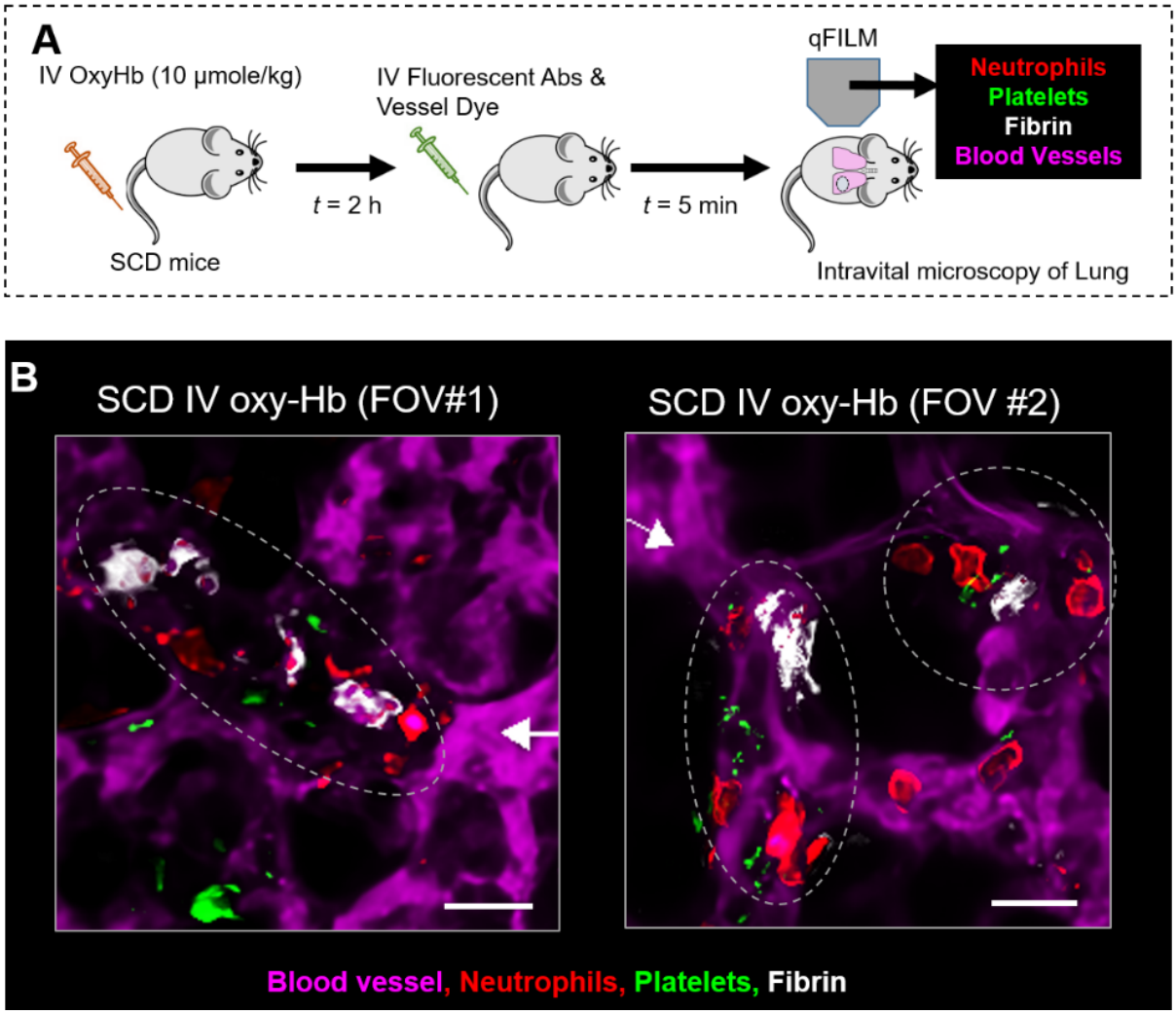

Supplemental Figure 4. Fibrin deposition contributes to lung vaso-occlusion in SCD mice *in vivo*. (A) Experimental scheme: SCD mice were IV administered 10 µmole/kg oxy-Hb and quantitative fluorescence intravital lung microscopy (qFILM) was used to assess the absence or presence of fibrin within the pulmonary microcirculation. Pulmonary microcirculation (pseudo-colored purple), neutrophils (red), platelets (pseudo-colored green), and fibrin (pseudo-colored white) were labeled *in vivo* by IV administration of FITC dextran, AF546-anti-Ly6G Ab, V450-anti-CD49b Ab, and AF647-anti-fibrin Ab, respectively. **(B)** Two representative qFILM images (field of views; FOVs) showing fibrin (white) present within and around the neutrophil-platelet

aggregates (marked with dotted ellipse) occluding the pulmonary arteriole bottle-necks in SCD mice administered IV Oxy-Hb. White arrows denote the direction of blood flow. Scale bars 20 μm.

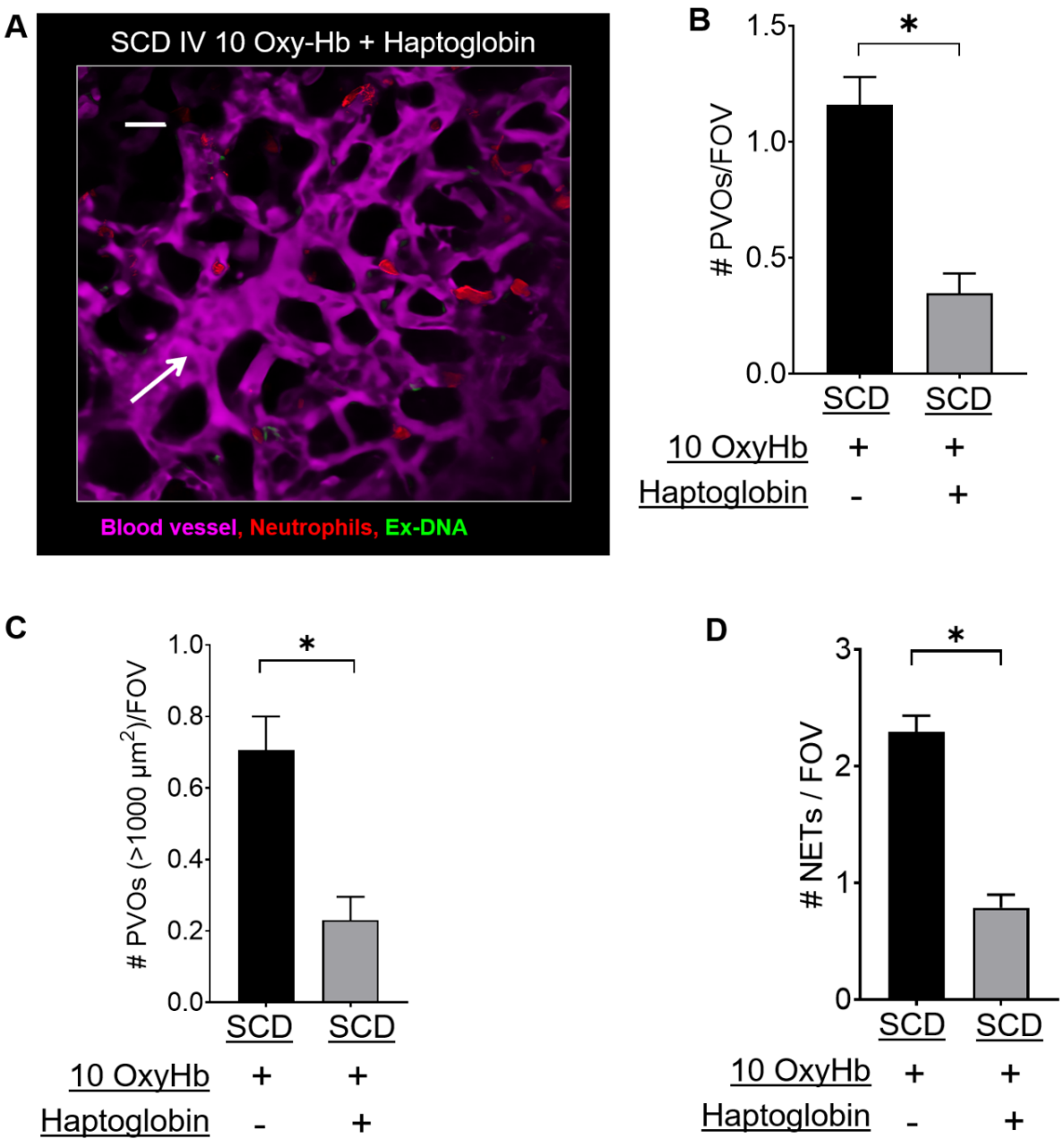

Supplemental Figure 5. Intravenous administration of haptoglobin attenuates vaso-occlusion and NETs in the lung of SCD mice *in vivo*. SCD mice were IV administered 10 µmole/kg oxy-Hb (10 oxy-Hb) without or with 10 µmole/kg haptoglobin. Quantitative fluorescence intravital lung microscopy (qFILM) was used to detect vaso-occlusion and NETs in the lung. Pulmonary microcirculation (pseudo-colored purple), neutrophils (pseudo-colored red) and extracellular DNA

(pseudo-colored green) were labeled *in vivo* by IV administration of FITC dextran, Pacific Blue-anti-Ly6G Ab and Sytox Orange, respectively. **(A)** Representative qFILM image shows absence of vaso-occlusion (neutrophil-aggregates absent in the pulmonary arteriole) and NETs (green staining absent) in the lung of an SCD mouse IV administered 10 oxy-Hb + haptoglobin. White arrow denotes the direction of blood flow within the pulmonary arteriole. Alveoli are marked with asterisks. Scale bar 20 μm. The diameter of pulmonary arteriole in is ~29 μm. Pulmonary vaso-occlusions (PVOs) were compared between treatment groups using following two parameters based on the strategy described in Supplemental Methods: Number of PVOs per Field of View (#PVOs/FOV) and number of large PVOs (with area > 1000 μm^2) per FOV. Both **(B)** #PVOs/FOV and **(C)** #PVOs (with area > 1000 μm^2) per FOV were significantly less in SCD mice IV administered 10 oxy-Hb + haptoglobin (n=4 mice; 52 FOVs) than SCD mice IV administered 10 oxy-Hb alone (n=5 mice; 75 FOVs). **(D)** NETs in the lung were quantified as described in the Supplemental Methods. Number of NETs per FOV (#NETs/FOV) were significantly less in SCD mice IV administered 10 oxy-Hb + haptoglobin (n=4 mice; 52 FOVs) than SCD mice IV administered 10 oxy-Hb alone (n=4 mice; 44 FOVs). Data represent Mean ± SE. Means compared using students *t*-test. * denotes $p < 0.05$. QFILM FOV size~65,536 μm^2.

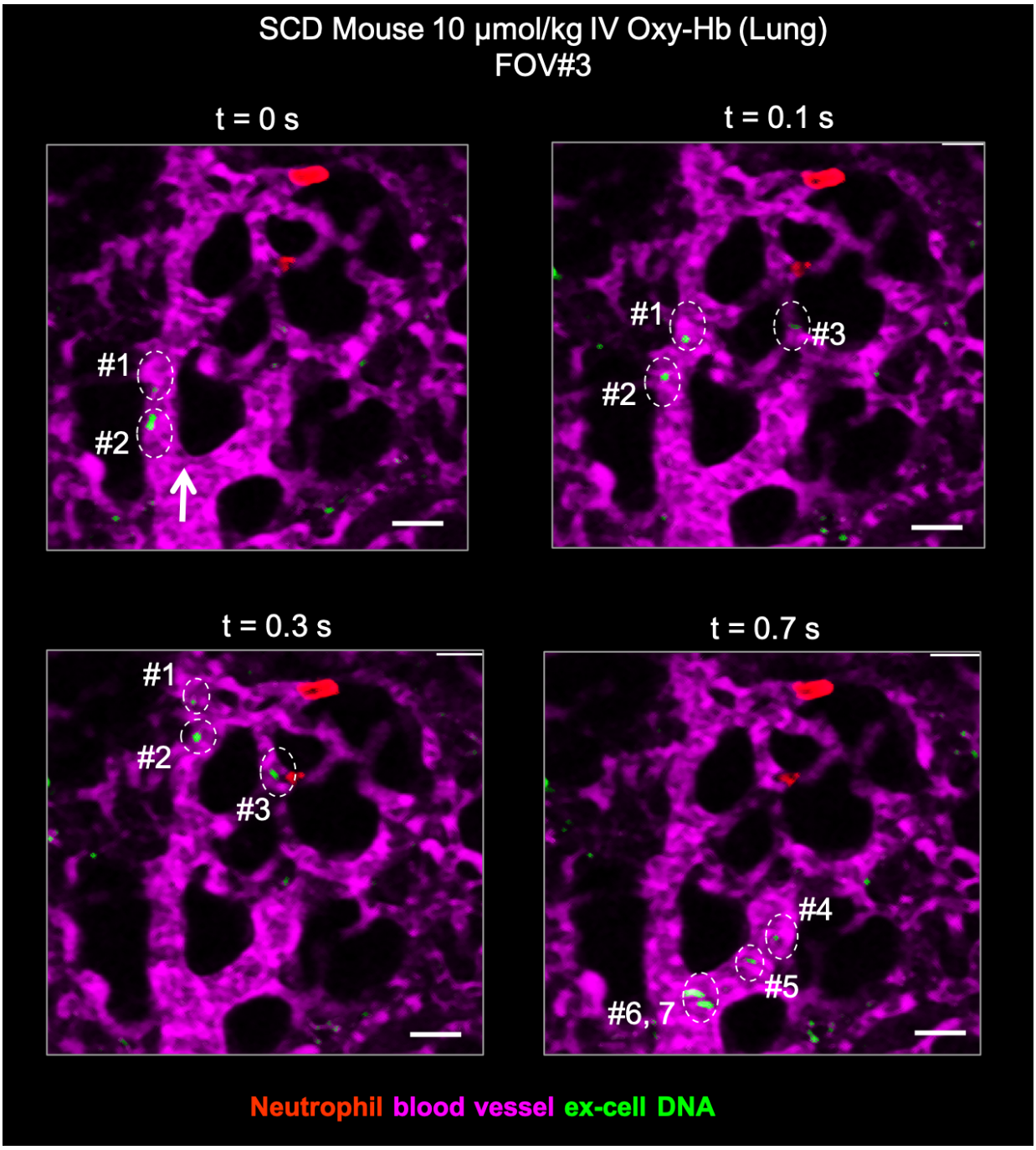

Supplemental Figure 6. Circulating NETs embolize to the lung from other organs in SCD mice *in vivo*. Experimental scheme shown in Figure 2A. SCD mouse intravenously (IV) administered 10 µmole/kg oxy-Hb and quantitative Fluorescence Intravital Lung Microscopy (qFILM) was used to assess the absence or presence of circulating NETs (cNETs) within the

pulmonary microcirculation. Pulmonary microcirculation (pseudo-colored purple), neutrophils (pseudo-colored red) and extracellular DNA (pseudo-colored green) were labeled *in vivo* by IV administration of FITC dextran, Pacific Blue-anti-Ly6G Ab and Sytox Orange, respectively. Third representative qFILM FOV showing several cNETs (green fragments marked with white ovals) entering the lung microcirculation (purple) *via* the pulmonary arteriole at different time points. cNETs #1 and #2 entered the FOV *via* the pulmonary arteriole (diameter ~27.9 μm) at 0 s, cNET #3 entered the FOV at 0.1 s, cNETs #1, #2 and #3 left the FOV, while cNETs #4, #5, #6 and #7 entered the FOV at 0.7 s. Time points are relative to the first frame shown at $t = 0$ s. White arrows denote the direction of blood flow within the pulmonary arteriole. Scale bars 20 μm.

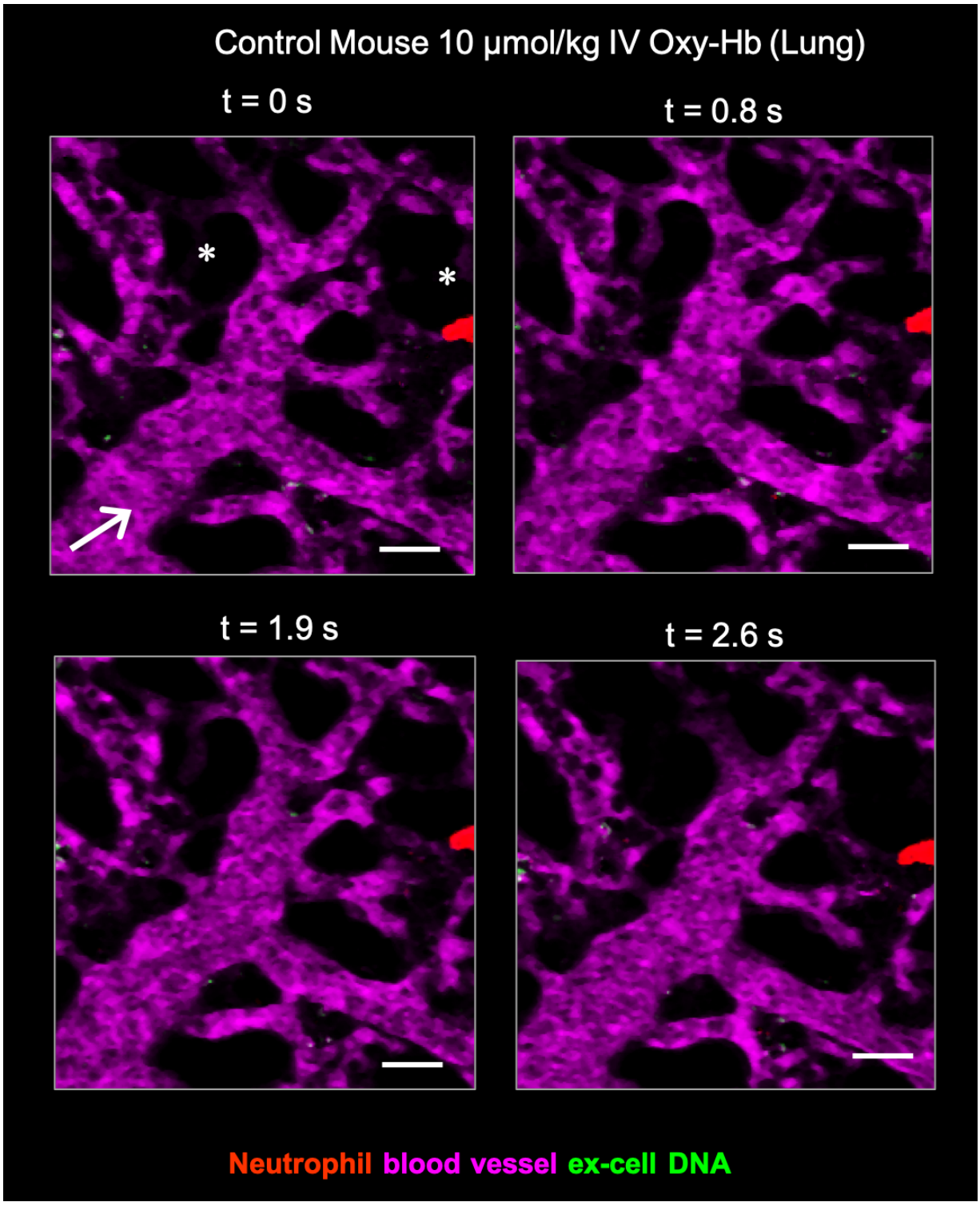

Supplemental Figure 7. Circulating NETs are absent in the lung microcirculation of control mice challenged with intravenous (IV) oxy-Hb. Experimental scheme shown in Figure 2A.

Control mouse administered 10 μmole/kg IV oxy-Hb and quantitative Fluorescence Intravital Lung Microscopy (qFILM) was used to assess the absence or presence of circulating NETs (cNETs) within the pulmonary microcirculation. Pulmonary microcirculation (pseudo-colored purple), neutrophils (pseudo-colored red) and extracellular DNA (pseudo-colored green) were labeled *in vivo* by IV administration of FITC dextran, Pacific Blue-anti-Ly6G Ab and Sytox Orange, respectively. Representative qFILM FOV shown at four different time points. cNETs (green) were not observed to enter the lung microcirculation of a control mouse administered IV oxy-Hb. Pulmonary arteriole diameter ~ 30.9 μm. Time points are relative to the first frame shown at t = 0 s. Complete time series shown in Video 10. White arrows denote the direction of blood flow within the pulmonary arteriole. Scale bars 20 μm. Alveoli marked with asterisks.

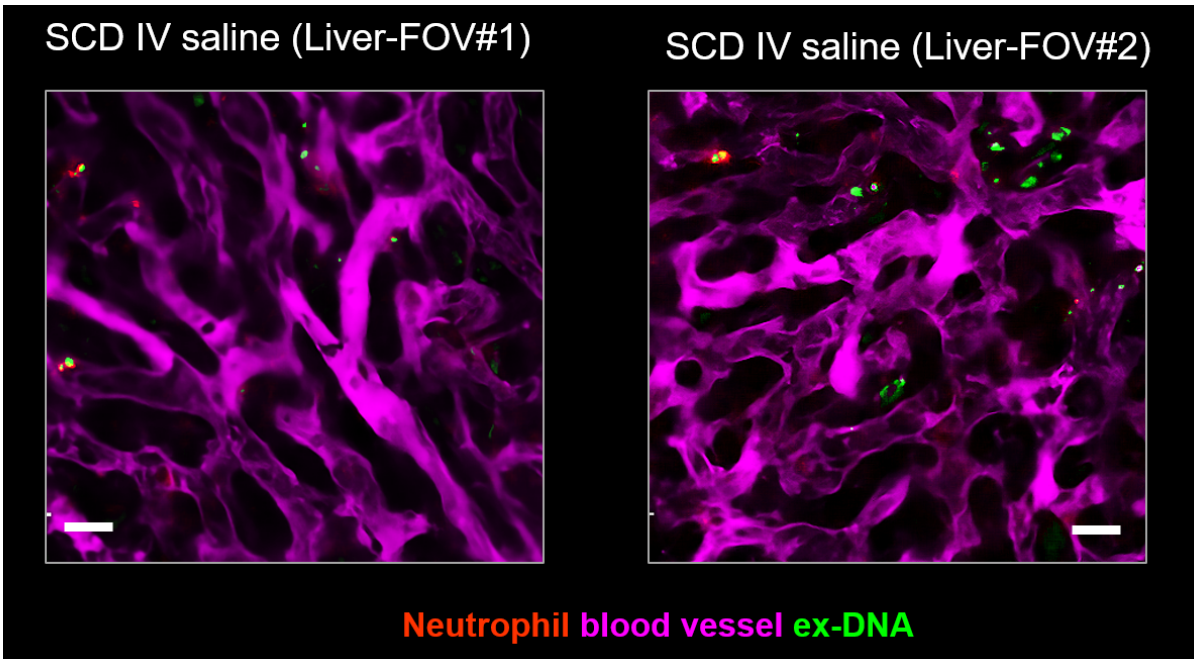

Supplemental Figure 8. NETs are rare in the liver of SCD mice administered IV saline. Experimental scheme shown in Figure 3A. SCD mice were IV administered saline. Intravital fluorescence microscopy was used to assess the absence or presence of NETs within the liver microcirculation. Microcirculation (pseudo-colored purple), neutrophils (pseudo-colored red) and extracellular DNA (pseudo-colored green) were labeled *in vivo* by IV administration of Texas-red dextran, Pacific Blue-anti-Ly6G Ab and Sytox Green, respectively. Two representative liver intravital microscopy images (Field of views; FOVs #1 and 2) are shown. NETs identified as neutrophils (red) releasing extracellular DNA (green) were rare in the liver microcirculation of SCD mice administered IV saline. Scale bars 20 μm.

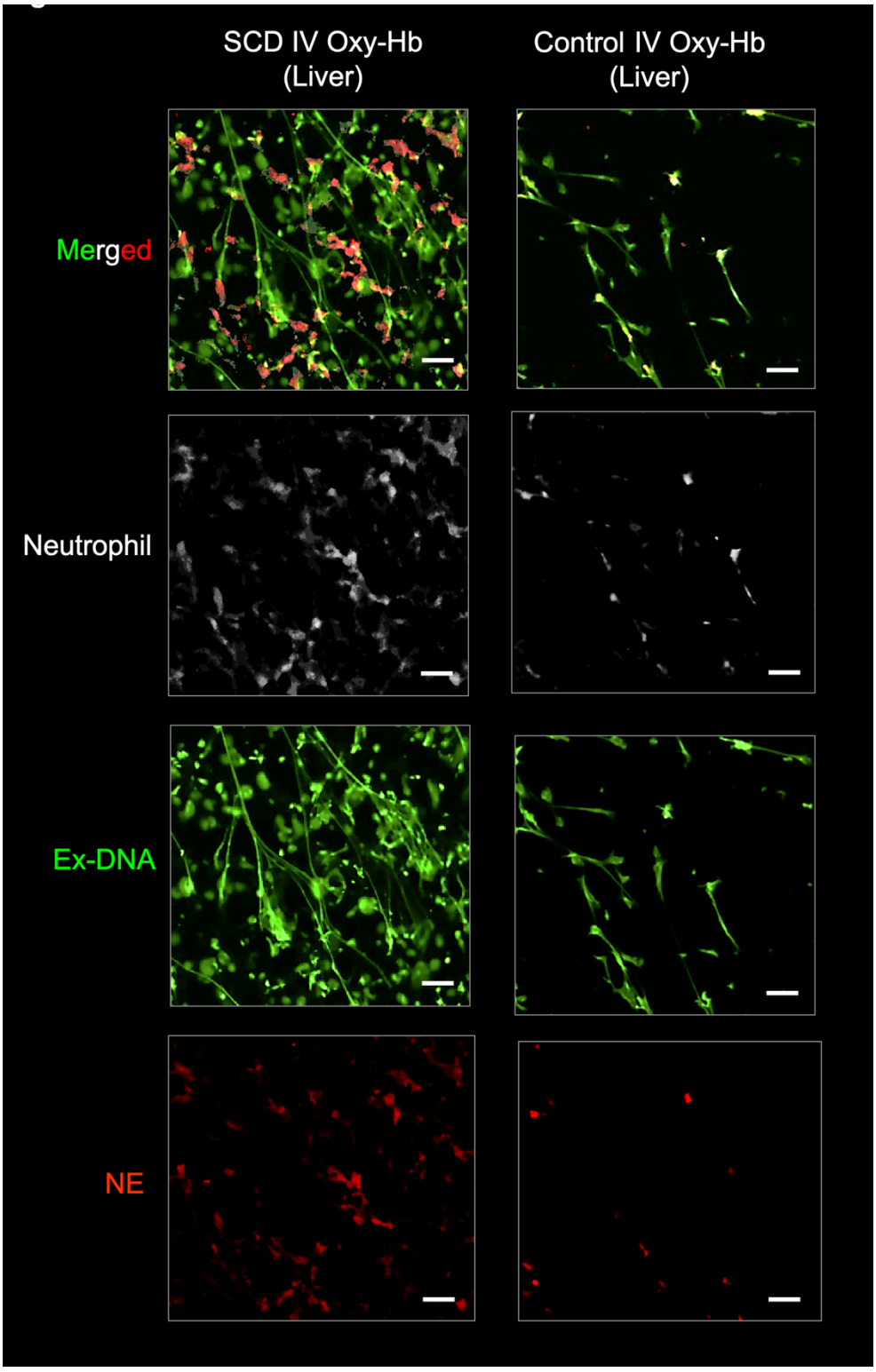

Supplemental Figure 9. NETs are abundant in the liver of SCD but not control mice challenged with intravenous (IV) oxy-Hb. Control or SCD mice were IV administered 10

μmole/kg oxy-Hb. Freshly cut-unfixed slices of excised liver were stained *in vitro* for neutrophils (Pacific Blue-anti-Ly6G Ab), extracellular DNA (Sytox Green), and neutrophil elastase (NE; AF546-anti-NE Ab), and confocal microscopy was used to identify NETs based on colocalization of DNA (green) with neutrophils (pseudo colored white) and NE (red). Representative confocal micrographs reveal abundance of NETs in the liver of an SCD but rare in the liver of control mouse administered IV oxy-Hb. NETs were identified as neutrophil-associated DNA strands positive for neutrophil-elastase (NE). Scale bar is 20 μm.

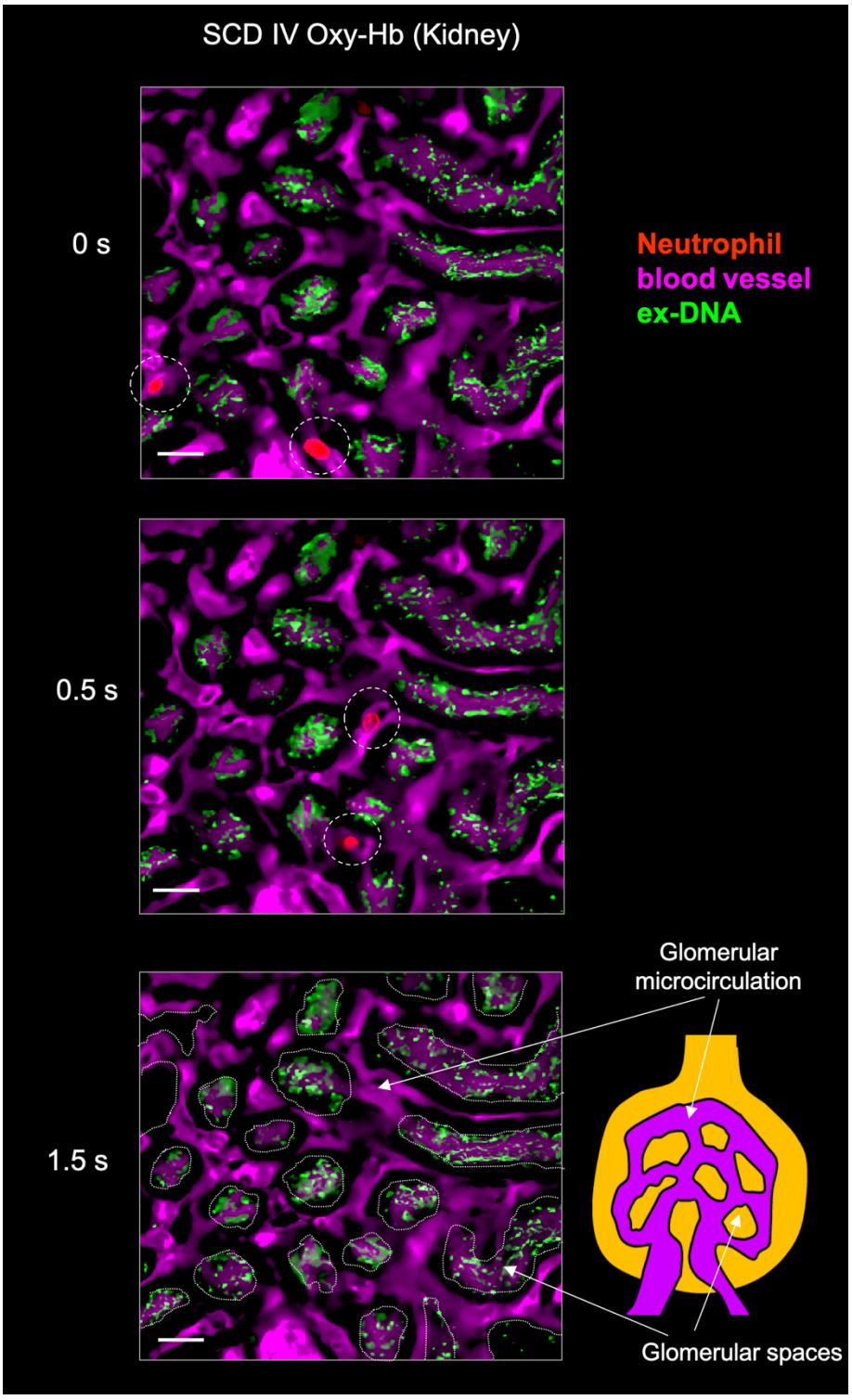

Supplemental Figure 10. NETs are rare in the kidney microcirculation of SCD mice challenged with intravenous (IV) oxy-Hb. SCD mice were IV administered 10 μmole/kg oxy-

Hb and intravital fluorescence microscopy was used to assess the absence or presence of NETs within the kidney microcirculation. Microcirculation (pseudo-colored purple), neutrophils (pseudo-colored red) and extracellular DNA (pseudo-colored green) were labeled *in vivo* by IV administration of FITC dextran, Pacific Blue-anti-Ly6G Ab and Sytox Orange, respectively. Refer Supplemental Methods for details. A representative kidney intravital microscopy FOV shown at three different time points and the corresponding Video 16 reveal four different neutrophils (red; marked with white dotted circles at 0 and 0.5 s) rapidly transiting (appearing and disappearing) through the kidney microcirculation (purple) in an SCD mouse administered IV oxy-Hb. The island like structures (outlined by white lines at 1.5 s) interspacing capillaries are glomerular spaces (see schematic in inset). Neither sequestered neutrophils nor any associated extracellular-DNA were present in kidney microcirculation, suggestive of the absence of NETs. The green staining in the FOV is primarily excess DNA dye (green) collecting in the glomerular spaces (islands outlined by white lines at 1.5 s) due to filtration across the blood-urine barrier. Scale bars 20 μm. Intravital kidney microscopy FOV size~65,536 μm^2.

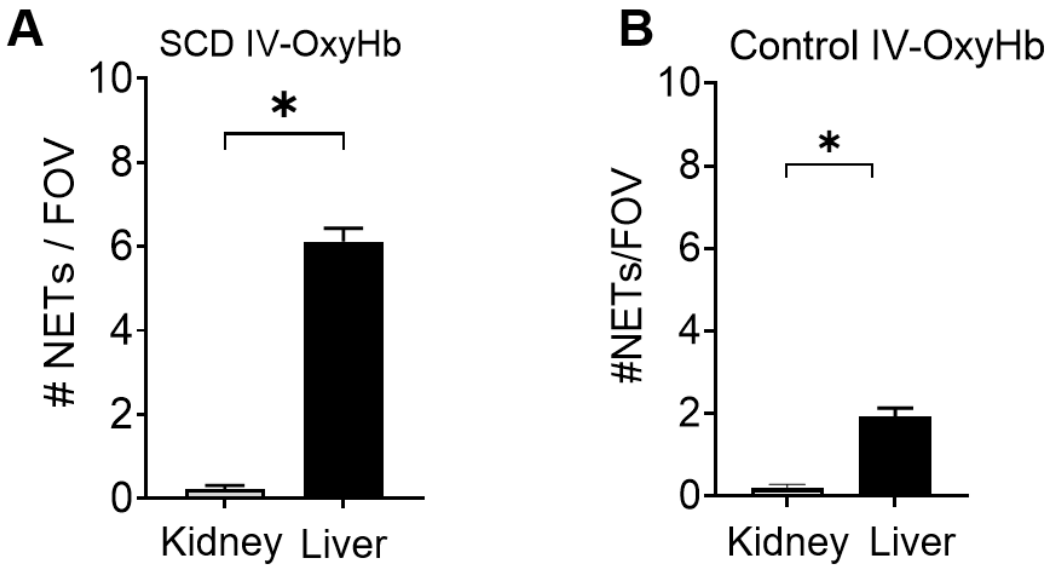

Supplemental Figure 11. Number of NETs in the liver vs kidney of SCD or control mice administered IV oxy-Hb. Intravital microscopy images were analyzed to compare number of NETs per FOV (#NETs/FOV) in the liver and kidney of SCD or control mice administered IV 10 μmole/kg oxy-Hb. **(A)** NETs were abundant (#NETs/FOV significantly higher by several folds) in the liver than kidney microcirculation of SCD mice administered IV oxy-Hb. **(B)** Unlike SCD mice, NETs were rare in both the liver and kidney (#NETs/FOV were few but still significantly more in the liver than kidney) of control mice administered IV oxy-Hb. SCD IV Oxy-Hb kidney (n=3 mice; 35 FOVs), SCD IV Oxy-Hb liver (n=4 mice; 44 FOVs), control IV Oxy-Hb kidney (n=3 mice; 16 FOVs), control IV Oxy-Hb liver (n=3 mice; 24 FOVs). Data represent Mean ± SE. Means compared using students *t*-test. * denotes $p < 0.05$. QFILM FOV size~65,536 μm^2.

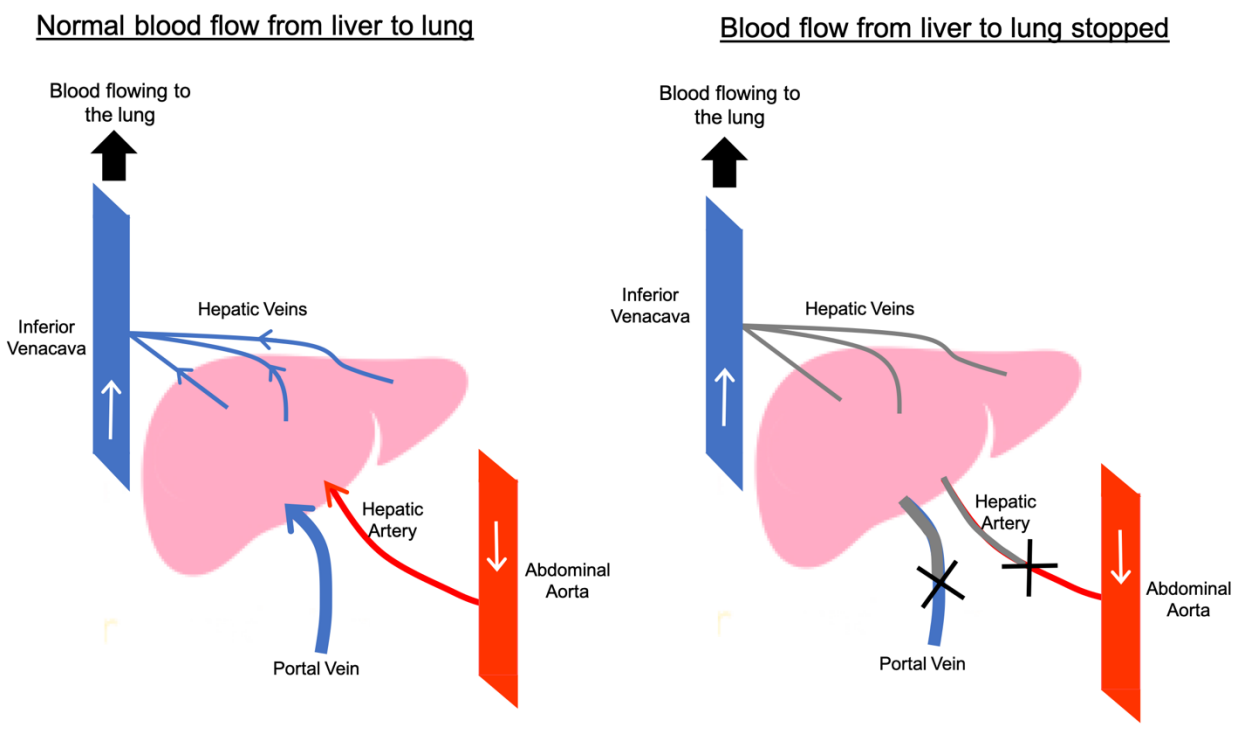

Supplemental Figure 12. Strategy used for stopping the blood flow from the liver to the lung. Under normal conditions, blood enters the liver through the hepatic artery and portal vein, travels through the liver sinusoids, and then exits through the multiple short branches of hepatic vein that drain into the Inferior-Vena-Cava (IVC). IVC carries blood to the right-heart and lung. In mice, the hepatic vein branches are short in length, primarily embedded inside the liver tissue, and drain individually into IVC, thus making it hard to clamp all of them simultaneously without causing trauma. Therefore, the blood flow through the liver to lung was stopped by simultaneously clamping the hepatic artery and portal vein using a silk suture ligature (right panel), which was confirmed using liver intravital microscopy as shown in Video 17.

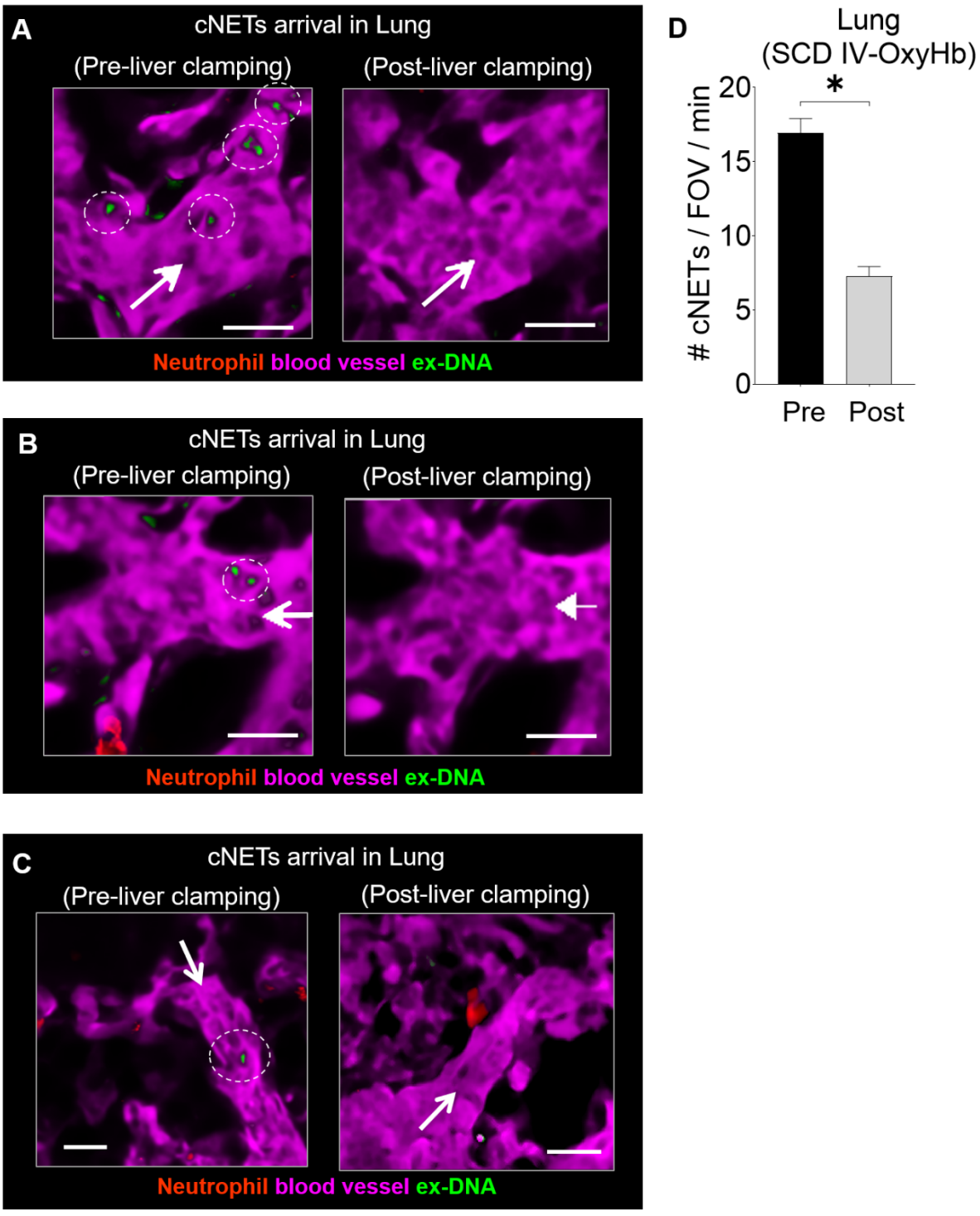

Supplemental Figure 13. Stopping the liver blood flow prevents arrival of cNETs in the lung. Quantitative Fluorescence Intravital Lung Microscopy (qFILM) was used to assess the effect of simultaneously ligating the hepatic artery and portal vein (liver clamping), on the arrival of

circulating NETs (cNETs) in the lung microcirculation of SCD mice administered IV oxy-Hb. **(A-C)** Three separate qFILM FOVs (**A** and **Video 25; B and Video 26; C and Video 18**) show cNETs (green; marked with dotted white circle) entering the pulmonary arteriole pre- but not post-clamping of liver blood flow. **(D)** Times-series of qFILM images were analyzed to quantify number of cNETs arriving in the lung per FOV over a 1-minute duration (#cNETs/FOV/min). #cNETs/FOV/min were significantly reduced (3-folds) following clamping of liver blood flow in SCD mice administered IV oxy-Hb (n=5 mice; 45 FOVs pre-clamp; 33 FOVs post clamp). FOV size~65,536 μm^2. Scale bars 20 μm. Data represents Mean ± SE and compared using Students *t*-test. * denotes $p < 0.05$. Arrow denotes the direction of blood flow.

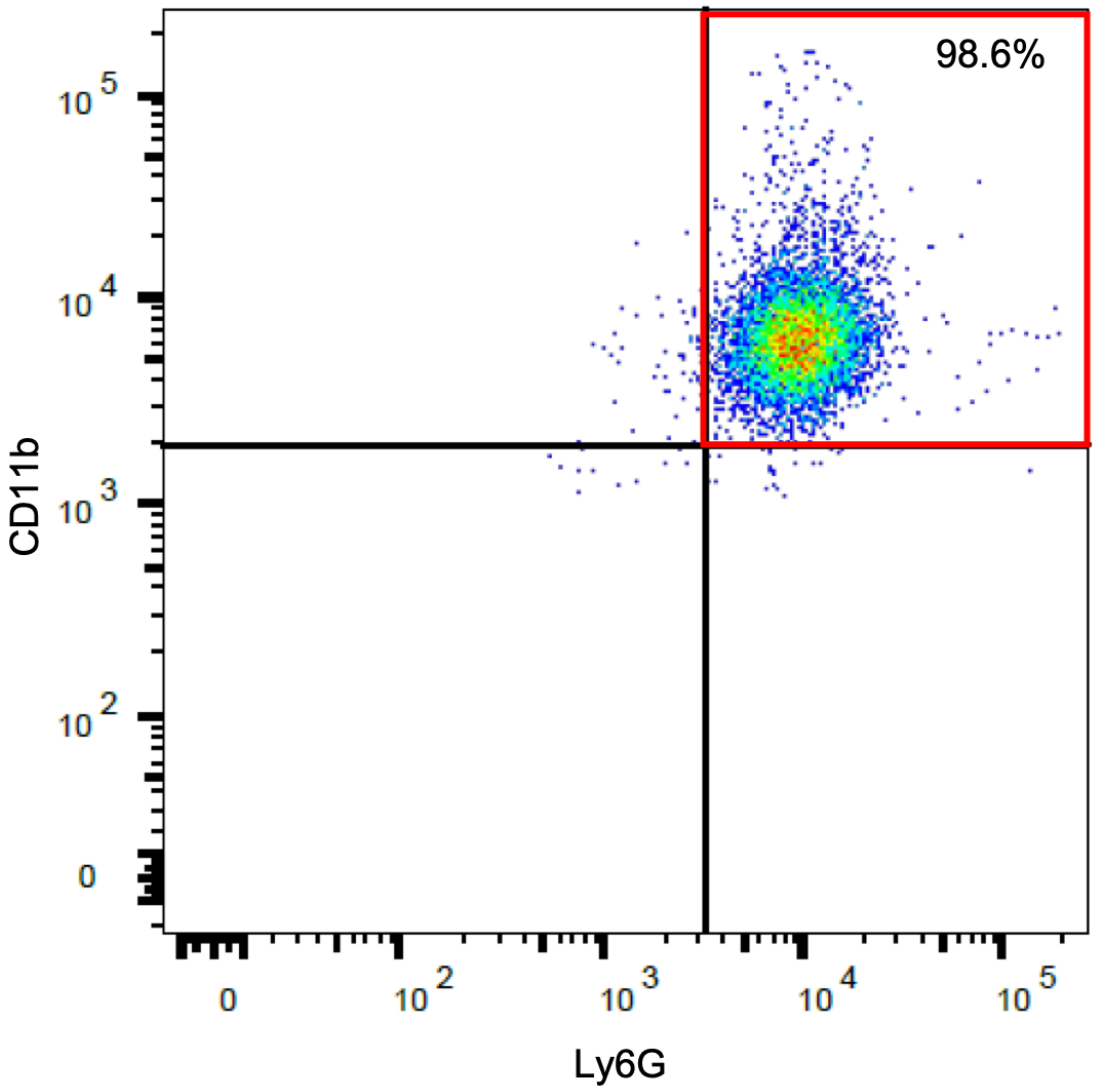

Supplemental Figure 14. Purity of murine neutrophils. Neutrophils were isolated from peripheral blood of mice using the negative selection approach and purity was determined using flow cytometry by identifying neutrophils as $CD11b^{+}/Ly6g^{+}$ dual positive cells. Refer Supplemental Methods for details. As shown in the representative flow cytometry plot, the purity of isolated murine neutrophils was always greater than 98%.

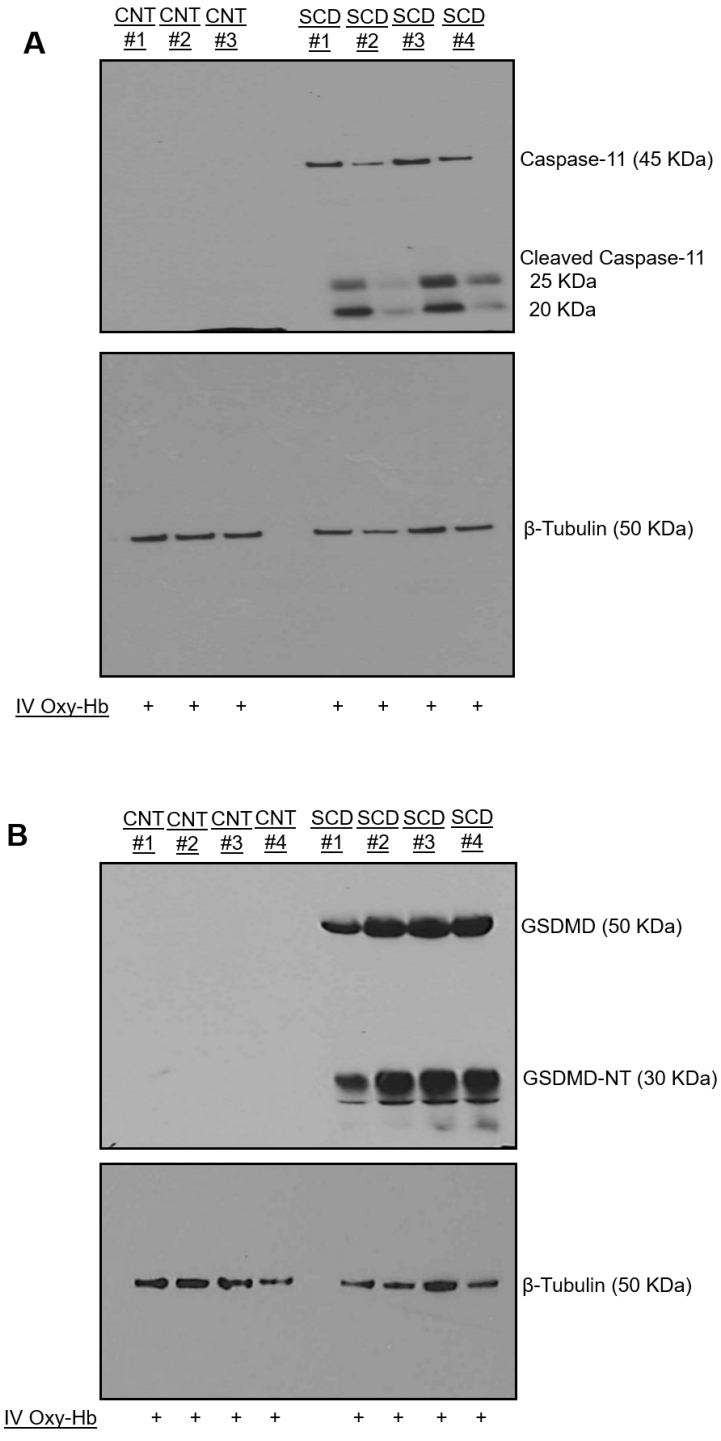

Supplemental Figure 15. Uncropped images of the western blot micrographs shown in Figure 4. (A) Uncropped images of western blot micrographs shown in Figure 4I. **(B)** Uncropped images of western blot micrographs shown in Figure 4L.

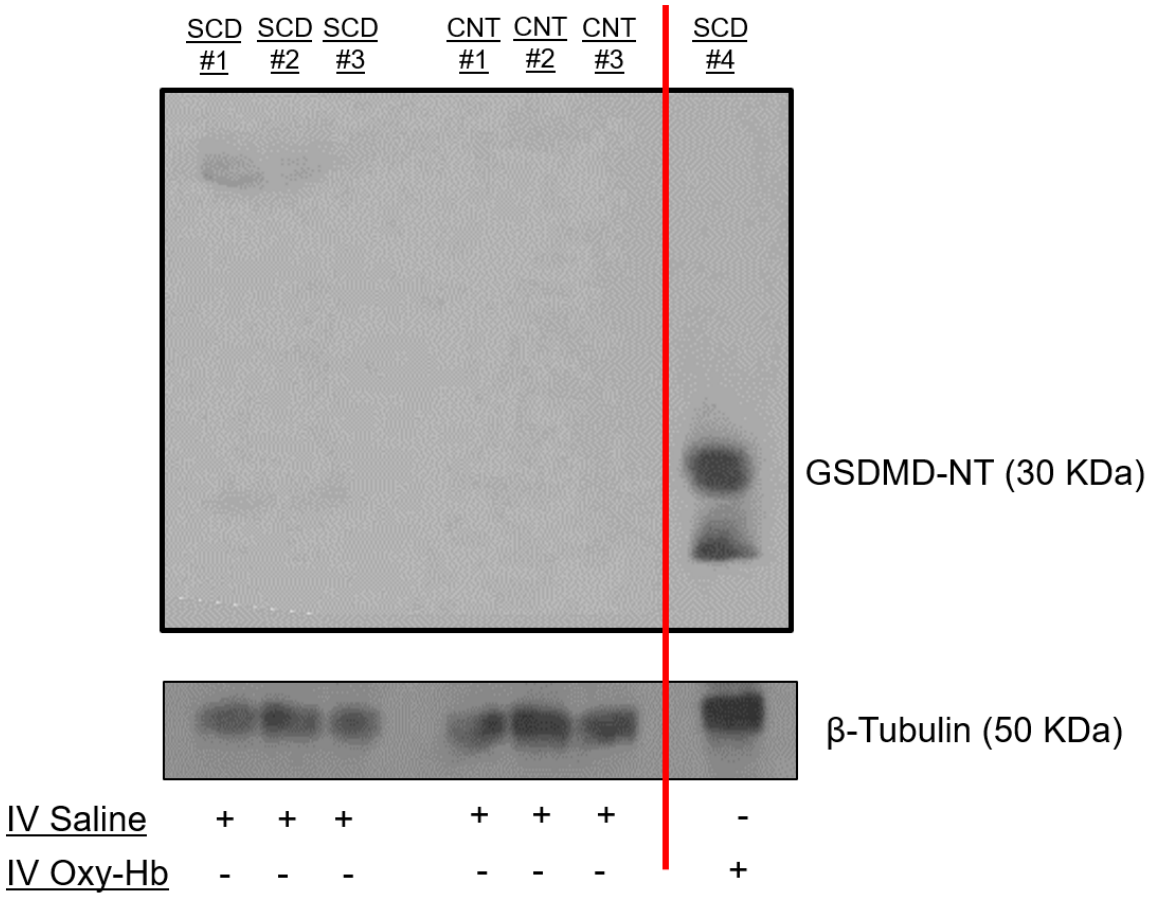

Supplemental Figure 16. GSDMD-NT is undetectable in SCD and control mice neutrophils at baseline. Control or SCD mice were IV administered saline, venous blood was collected 3 hours later, neutrophils were isolated from blood using a negative selection approach, purity confirmed (>98%) using flow cytometry, and neutrophils were used in western blot analysis. Refer to Supplemental Methods for details. Expression of cleaved N-terminus domain of Gasdermin-D (GSDMD-NT; 30 kDa) was below the detection limit in neutrophils of SCD or control mice IV administered saline. Neutrophils from an SCD mouse IV administered 10 μmole/kg oxy-hemoglobin shown as a positive control (GSDMD-NT bands present) in the last lane (right of red line) for comparison. β-tubulin (50 kDa) was the loading control. Each lane represents a separate mouse. CNT, Control mouse. SCD, SCD mouse.

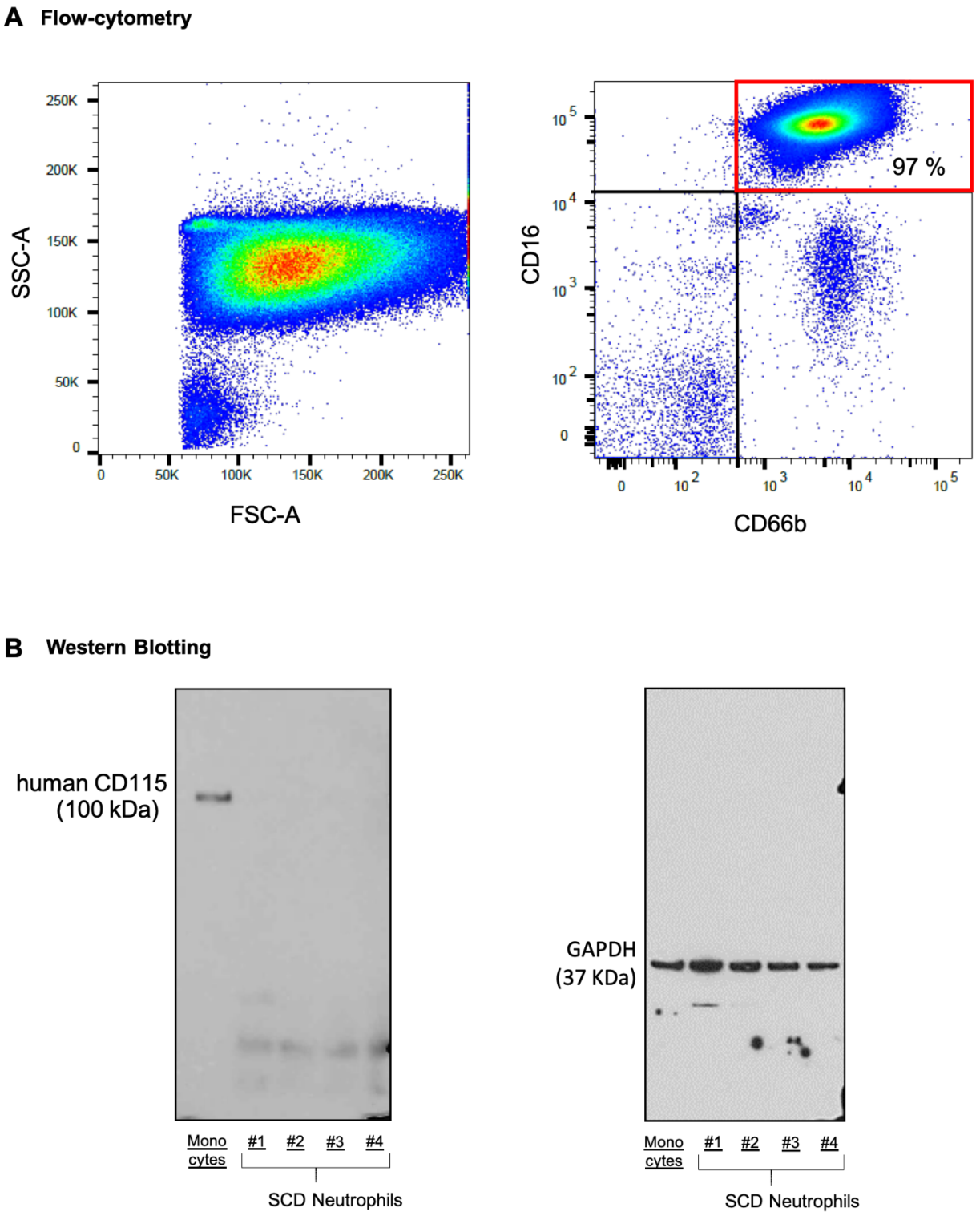

Supplemental Figure 17. Purity of human neutrophils. Neutrophils were isolated from peripheral blood of human subjects using the strategy described in Methods and purity was

confirmed using flow cytometry and western blot analysis. **(A)** Flow cytometry-human neutrophils were identified as cells dual positive for CD16 and CD66b. Neutrophil purity was found to be ~ 97%. **(B)** Western blot- CD115 (~100 kDa; monocyte marker) was used to detect contamination by monocytes. Isolated human monocytes were used as a positive control. CD115 was present in human monocyte lysate (lane 1) but absent in the lysates of neutrophils isolated from peripheral blood of four SCD patients (lane 2-5), confirming lack of monocyte contamination. Right side of Panel B shows the loading control – GAPDH (37 kDa) for the monocyte and four neutrophil samples.

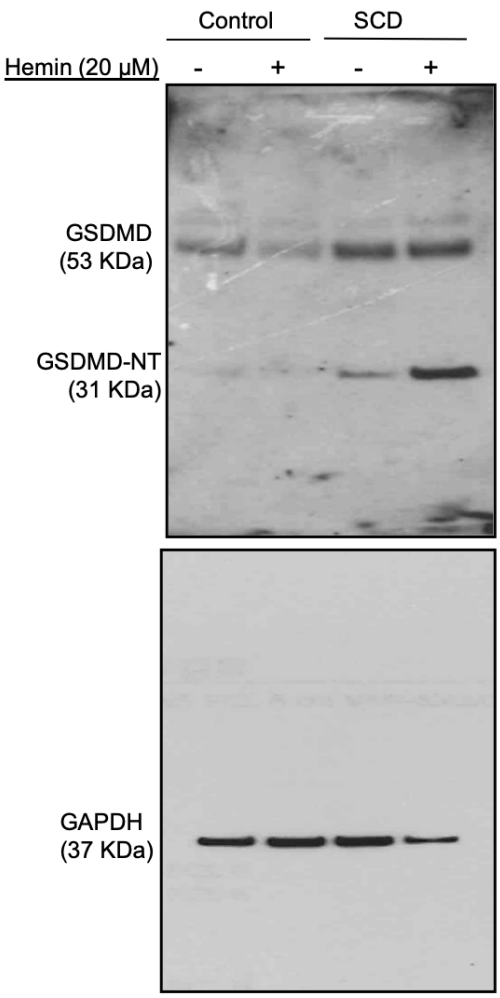

Supplemental Figure 18. Uncropped images of the western blot micrographs shown in Figure 5B.

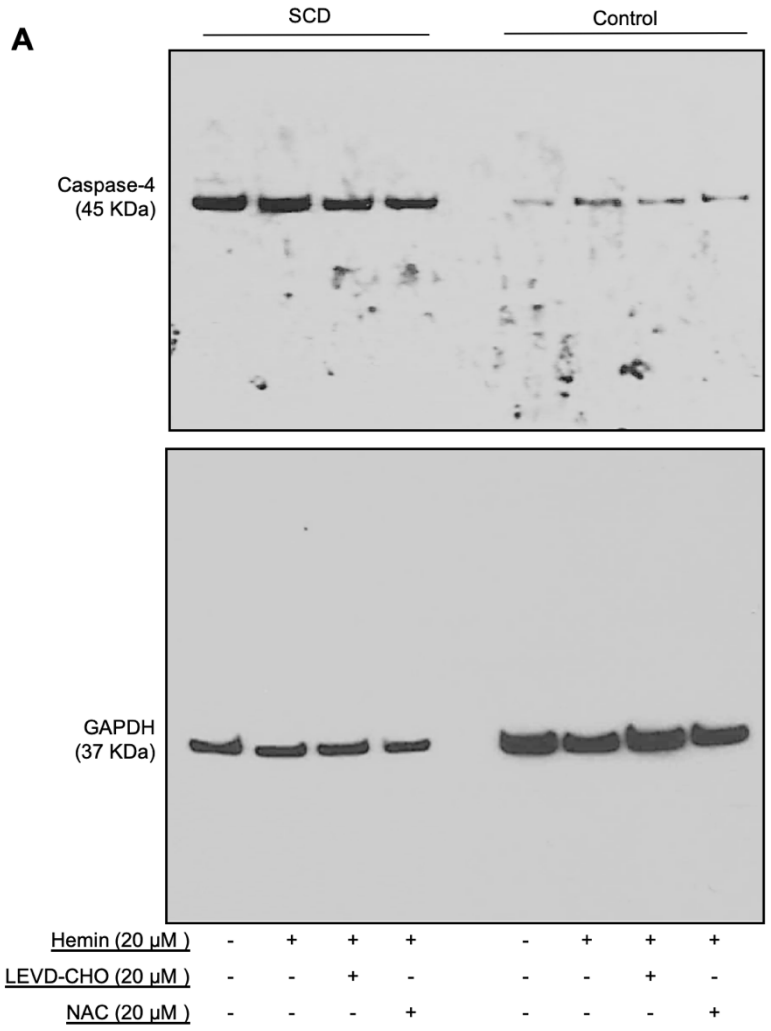

Supplemental Figure 19. Uncropped images of the western blot micrographs shown in Figure 5H.

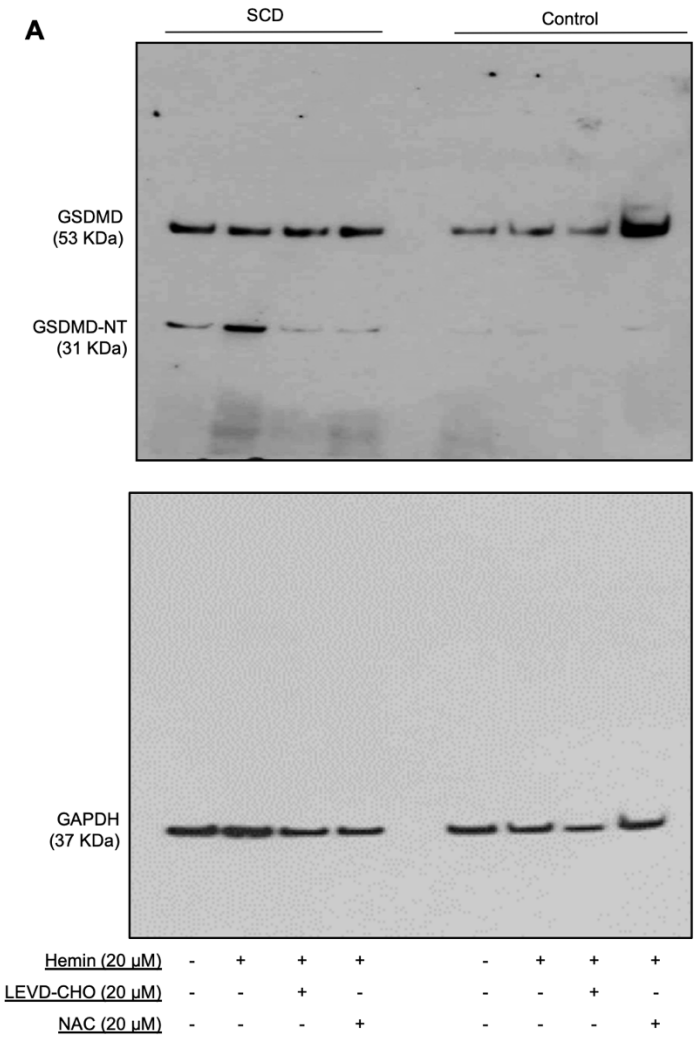

Supplemental Figure 20. Uncropped images of the western blot micrographs shown in Figure 5L.

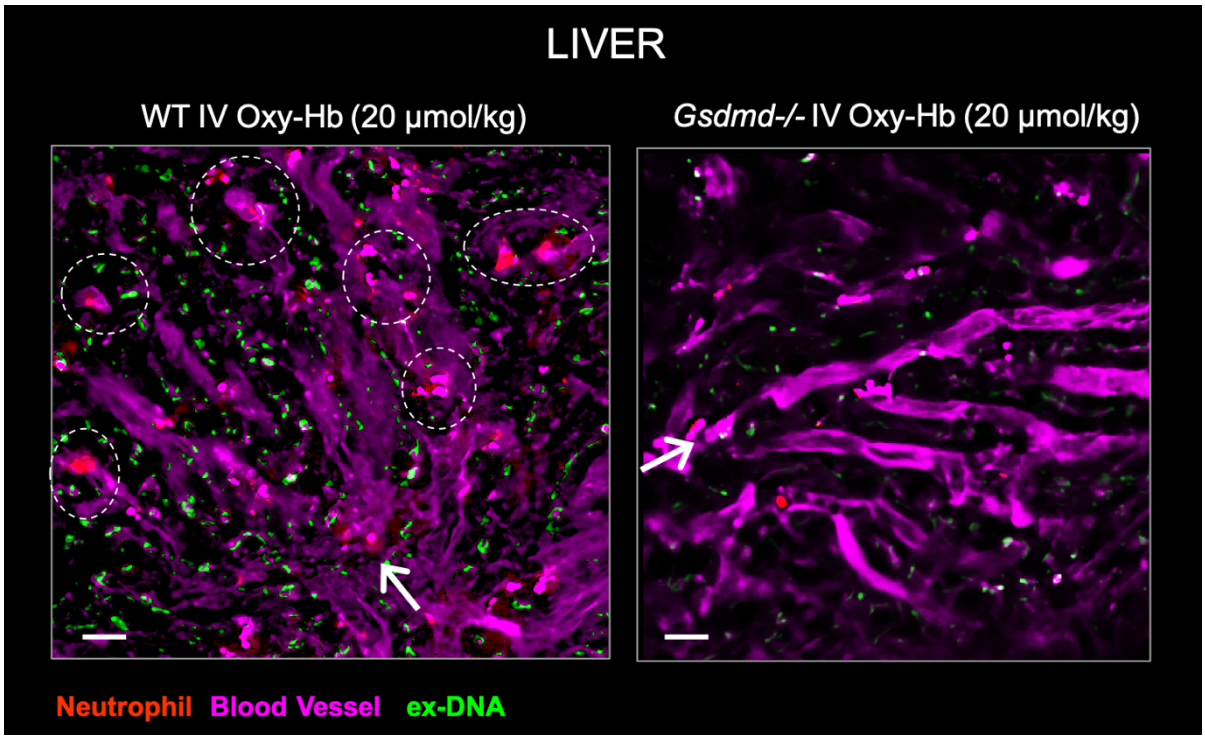

Supplemental Figure 21. Intravenous administration of 20 µmol/kg oxy-Hb triggered NETs generation in the liver of wild-type but not *Gsdmd*$^{-/-}$ mice. Experimental scheme is shown in Figure 6E. WT or *Gsdmd*$^{-/-}$ mice were IV administered 20 µmole/kg oxy-Hb. Microcirculation, neutrophils and extracellular DNA were labeled *in vivo* by IV administration of Texas-red dextran, Pacific Blue-anti-Ly6G Ab and Sytox Green, respectively, and intravital fluorescence microscopy was used to assess the absence or presence of NETs within the liver microcirculation of live mice. Representative liver intravital microscopy images show numerous NETs (marked with dotted ellipses) present in the liver of a WT mouse but absent in the *Gsdmd*$^{-/-}$ mouse. NETs were identified based on colocalization of neutrophil (pseudo-colored red) and extracellular DNA (green) in liver microcirculation (pseudo-colored purple). Scale bars 20 µm. Arrow denotes the direction of blood flow. Intravital liver microscopy FOV size~65,536 µm^2.

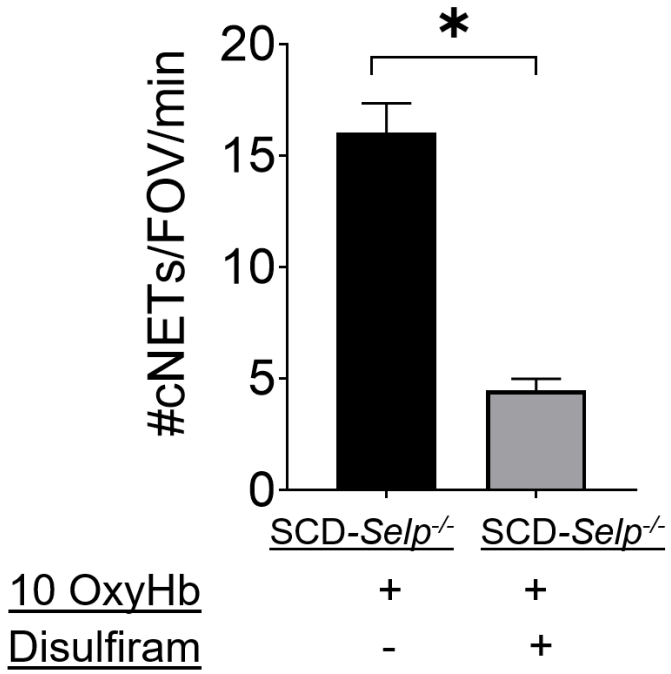

Supplemental Figure 22. GSDMD-inhibition prevents arrival of circulating NETs in the lung of *SCD-Selp*$^{-/-}$ mice *in vivo*. SCD-*Selp*$^{-/-}$ mice were IV administered 10 µmole/kg oxy-Hb (10 oxy-Hb) without or with 10 mg/kg GSDMD inhibitor (Disulfiram[14]). Microcirculation, neutrophils and extracellular DNA were labeled *in vivo* by IV administration of FITC dextran, Pacific Blue-anti-Ly6G Ab and Sytox Orange, respectively, and quantitative fluorescence intravital lung microscopy (qFILM) was used to detect arrival of circulating NETs (cNETs) within the lung microcirculation. QFILM images were analyzed as in Figure 2 to estimate number of cNETs entering per FOV in the lung over a 1-minute duration (#cNETs/FOV/min). #cNETs/FOV/min in the lung were significantly less (4-folds) in SCD-*Selp*$^{-/-}$ mice IV administered 10 oxy-Hb + Disulfiram (n=3 mice; 43 FOVs) than 10 oxy-Hb alone (n=5 mice; 71 FOVs). Data represents Mean ± SE and compared using Students *t*-test. * denotes $p < 0.05$. FOV size~65,536 µm^2.

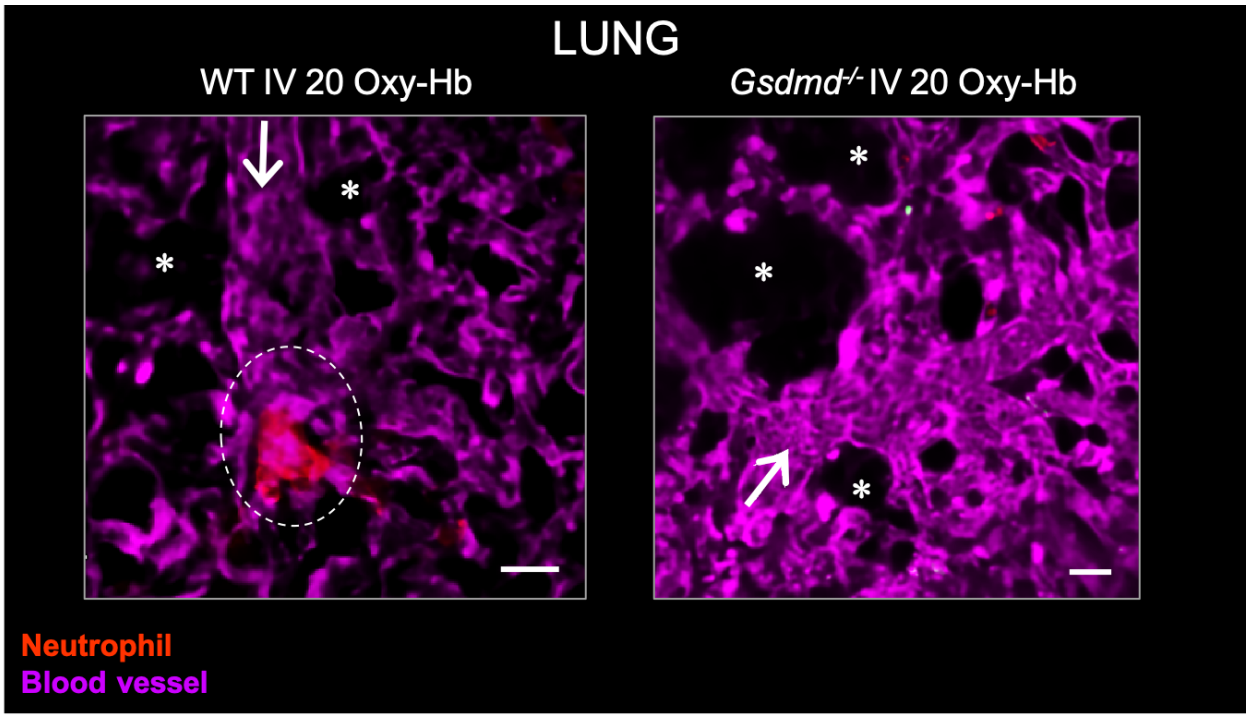

Supplemental Figure 23. Intravenous administration of 20 µmol/kg oxy-Hb triggered lung vaso-occlusion in wild-type but not *Gsdmd*$^{-/-}$ mice. Experimental scheme is shown in Figure 7A. Litter-mate wild type (WT) or *Gsdmd*$^{-/-}$ mice were intravenously (IV) administered 20 µmole/kg oxy-Hb (20 oxy-Hb). Quantitative fluorescence intravital lung microscopy (qFILM) was used to assess the absence or presence of pulmonary vaso-occlusion. Pulmonary microcirculation (pseudo-colored purple) and neutrophils (red). Representative qFILM images show a large neutrophil aggregate (marked with dotted ellipse) occluding the arteriolar bottle-neck in the lung of a WT mouse (left panel) given IV 20 oxy-Hb, while such aggregates were absent in the lung microcirculation of a *Gsdmd*$^{-/-}$ mouse (right panel) given IV 20 oxy-Hb. White arrows denote the direction of blood flow within the pulmonary arterioles. Alveoli are marked with asterisks. Scale bars 20 µm. The diameter of pulmonary arteriole in left and right panel is 28.6 and 31.8 µm, respectively. qFILM FOV size~65,536 µm^2.

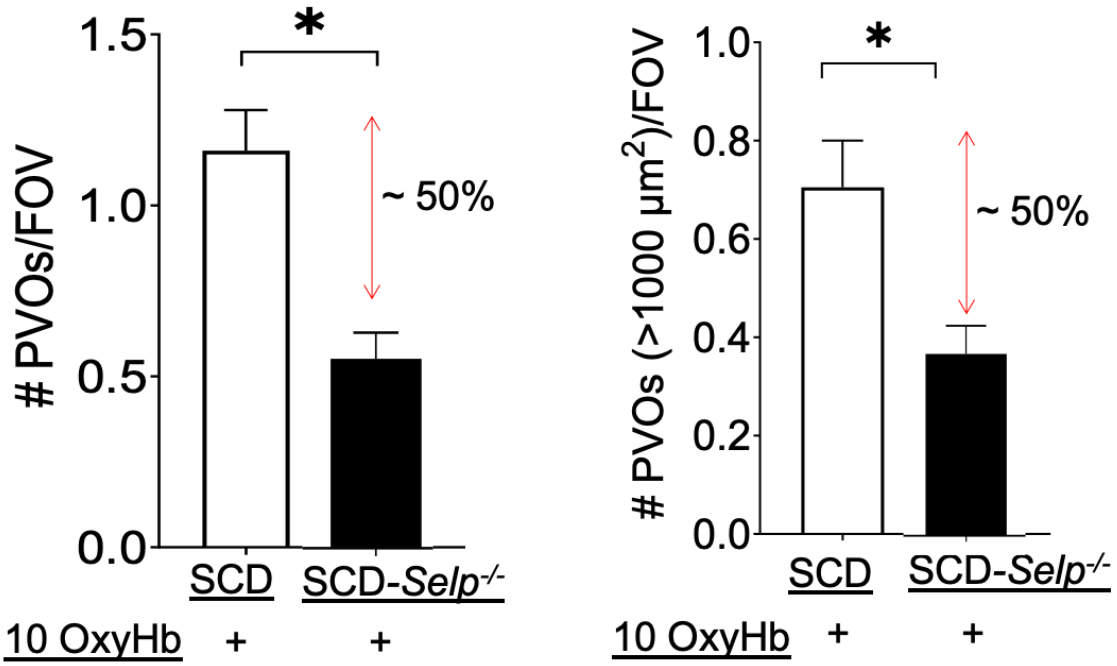

Supplemental Figure 24. P-selectin deficiency attenuates lung vaso-occlusion by ~50% in SCD mice. SCD or SCD-*Selp*$^{-/-}$ mice were intravenously (IV) administered 10 µmole/kg oxy-Hb (10 oxy-Hb). Quantitative fluorescence intravital lung microscopy (qFILM) was conducted to assess the absence or presence of pulmonary vaso-occlusion. Time-series of qFILM images were analyzed to quantify and compare pulmonary vaso-occlusions (PVOs) between treatment groups using following two parameters: Number of PVOs per Field of View (#PVOs/FOV) and number of large PVOs (with area > 1000 µm^2) per FOV. Refer Supplemental Methods for details. Both #PVOs/FOV and #PVOs (with area > 1000 µm^2) per FOV were (significantly) reduced by ~50% in SCD-*Selp*$^{-/-}$ (n=5 mice; 69 FOVs) than SCD mice (n=5 mice; 75 FOVs) IV administered 10 oxy-Hb. qFILM FOV size~65,536 µm^2. Data represents Mean ± SE and compared using Students *t*-test. * denotes $p < 0.05$.

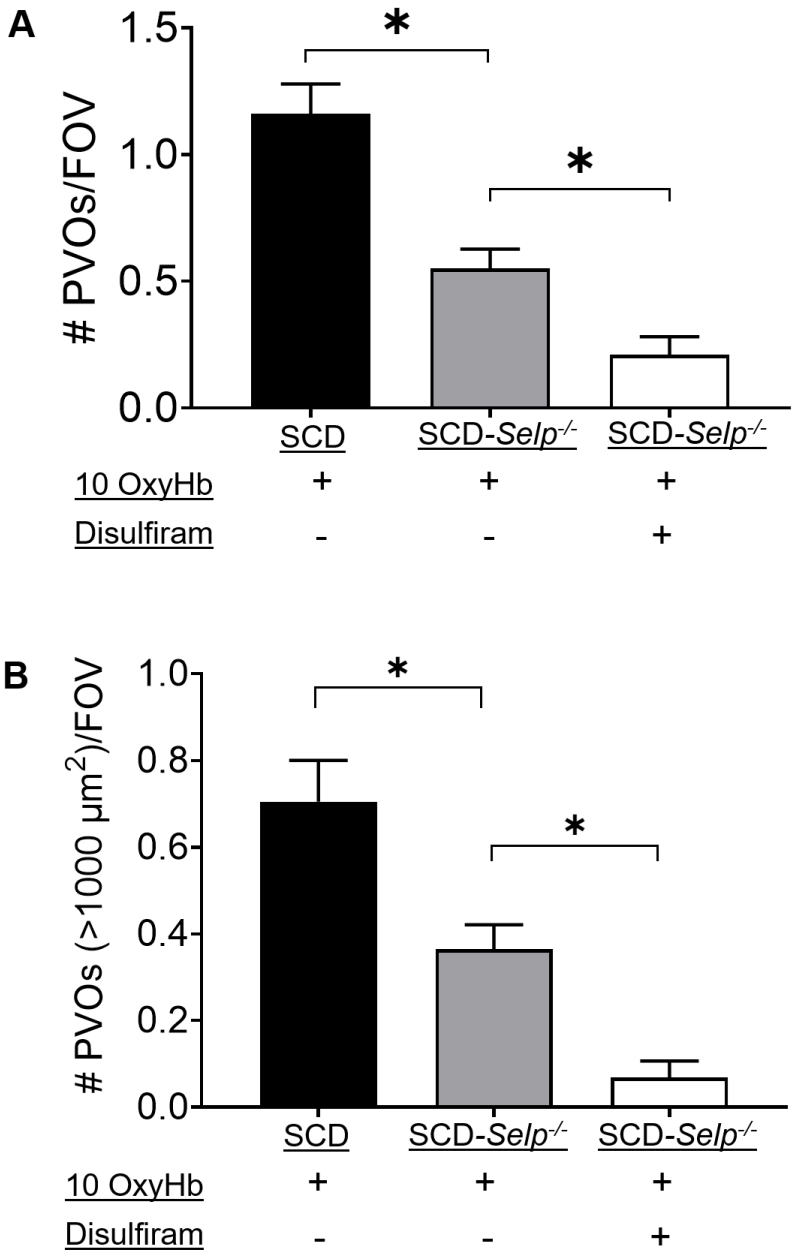

Supplemental Figure 25. Inhibiting GSDMD-pathway ameliorates P-selectin-independent lung vaso-occlusion in SCD. SCD-*Selp*$^{-/-}$ mice were IV administered 10 µmole/kg oxy-Hb (10 oxy-Hb) without or with 10 mg/kg GSDMD inhibitor (Disulfiram[14]). Quantitative fluorescence intravital lung microscopy (qFILM) was used to assess the absence or presence of pulmonary vaso-occlusion using the same experimental scheme described in Figure 7A. Pulmonary vaso-occlusions (PVOs) were compared between treatment groups using following two parameters:

Number of PVOs per Field of View (#PVOs/FOV) and number of large PVOs (with area > 1000 μm^2) per FOV. **(A)** #PVOs/FOV were significantly reduced and **(B)** #PVOs (with area > 1000 μm^2) per FOV were absent in SCD-*Selp*$^{-/-}$ mice IV administered 10 oxy-Hb + Disulfiram (white bar; n=3 mice; 43 FOVs) compared to SCD-*Selp*$^{-/-}$ mice IV administered 10 oxy-Hb alone (grey bar; n=5 mice; 69 FOVs). The data for SCD mice IV administered 10 oxy-Hb (n=5 mice; 75 FOVs) is included as black bars in A and B for relative comparison. FOV size~65,536 μm^2. Data represents Mean ± SE and compared using one-way ANOVA with Games-Howell's multiple comparisons test. * denotes $p < 0.05$.

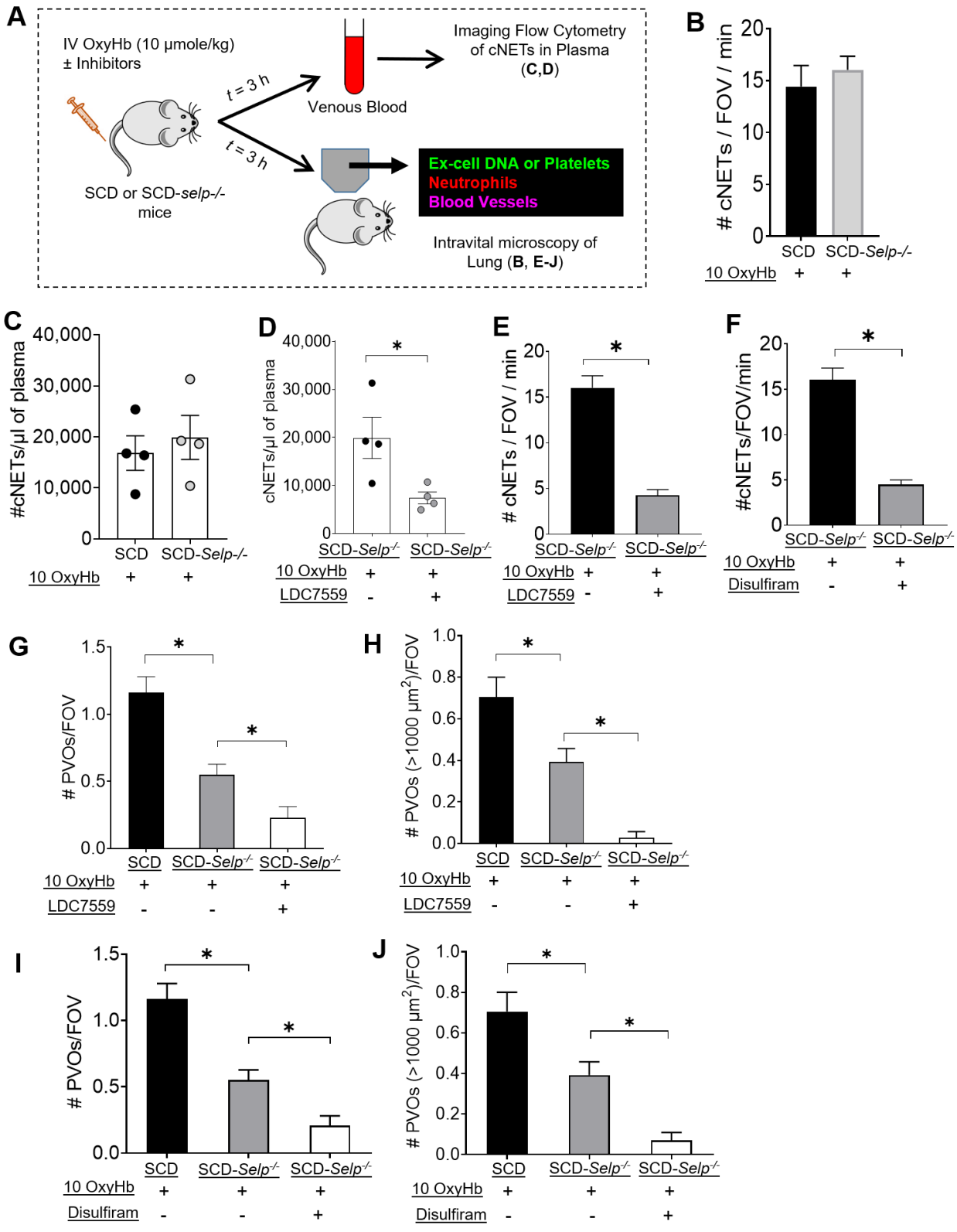

Supplemental Figure 26. GSDMD promotes NETs generation and lung vaso-occlusion in

SCD in a P-selectin-independent manner. (A) Experimental scheme: SCD or SCD-*Selp*$^{-/-}$ mice were IV administered 10 μmole/kg oxy-Hb (10 oxy-Hb) without or with 10 mg/kg GSDMD inhibitors LDC7559[1] or Disulfiram[14]. In C-D, venous blood was processed to generate PPP and cNETs detected in PPP using Imaging Flow Cytometry. Imaging Flow Cytometry data was quantified as described in Supplemental Methods to estimate concentration of cNETs (#cNETs/μl of plasma). In B,E-F, quantitative fluorescence intravital lung microscopy (qFILM) was used to detect arrival of circulating NETs (cNETs) within the lung microcirculation using the experimental strategy described in Figure 2. Number of cNETs entering per FOV over a 1-minute duration (#cNETs/FOV/min) were quantified using strategy described in Supplemental Methods. In G-J, qFILM was used to assess the absence or presence of pulmonary vaso-occlusion using the experimental strategy described in Figure 7A. Pulmonary vaso-occlusions (PVOs) were compared between treatment groups using following two parameters: Number of PVOs per Field of View (#PVOs/FOV) and number of large PVOs (with area > 1000 μm^2) per FOV. **(B)** #cNETs/FOV/min in SCD mice IV administered 10 oxy-Hb were not different from SCD-*Selp*$^{-/-}$ mice IV administered 10 oxy-Hb. SCD IV Oxy-Hb (n=4 mice; 44 FOVs). SCD-*Selp*$^{-/-}$ IV oxy-Hb (n=5 mice; 71 FOVs). **(C)** Plasma concentration of cNETs was not different between SCD and SCD-*Selp*$^{-/-}$ mice (n=4 mice per group) IV administered 10 oxy-Hb. **(D)** Plasma concentration of cNETs was significantly less in SCD-*Selp*$^{-/-}$ mice IV administered 10 oxy-Hb + LDC7559 (n=4 mice) than 10 oxy-Hb alone (n=4 mice). **(E)** #cNETs/FOV/min in the lung were significantly less (4-folds) in SCD-*Selp*$^{-/-}$ mice IV administered 10 oxy-Hb + LDC7559 (n=3 mice; 35 FOVs) than 10 oxy-Hb alone (n=5 mice; 71 FOVs). **(F)** #cNETs/FOV/min in the lung were significantly less (4-folds) in SCD-*Selp*$^{-/-}$ mice IV administered 10 oxy-Hb + Disulfiram (n=3 mice; 43 FOVs) than 10 oxy-Hb alone (n=5 mice; 71 FOVs). **(G)** #PVOs/FOV were significantly reduced and **(H)** #PVOs (with area > 1000 μm^2)

per FOV were absent in SCD-*Selp*$^{-/-}$ mice IV administered 10 oxy-Hb + LDC7559 (white bars; n=3 mice; 35 FOVs) compared to SCD-*Selp*$^{-/-}$ mice IV administered 10 oxy-Hb alone (grey bars; n=5 mice; 69 FOVs). **(I)** #PVOs/FOV were significantly reduced and **(J)** #PVOs (with area > 1000 μm^2) per FOV were absent in SCD-*Selp*$^{-/-}$ mice IV administered 10 oxy-Hb + Disulfiram (white bar; n=3 mice; 43 FOVs) compared to SCD-*Selp*$^{-/-}$ mice IV administered 10 oxy-Hb alone (grey bar; n=5 mice; 69 FOVs). The data for SCD mice IV administered 10 oxy-Hb (n=5 mice; 75 FOVs) is included as black bars in G-J for relative comparison. FOV size~65,536 μm^2. Data represents Mean ± SE and compared using Students *t*-test (B-F) or one-way ANOVA with Games-Howell's multiple comparisons test (G-J). * denotes $p < 0.05$.

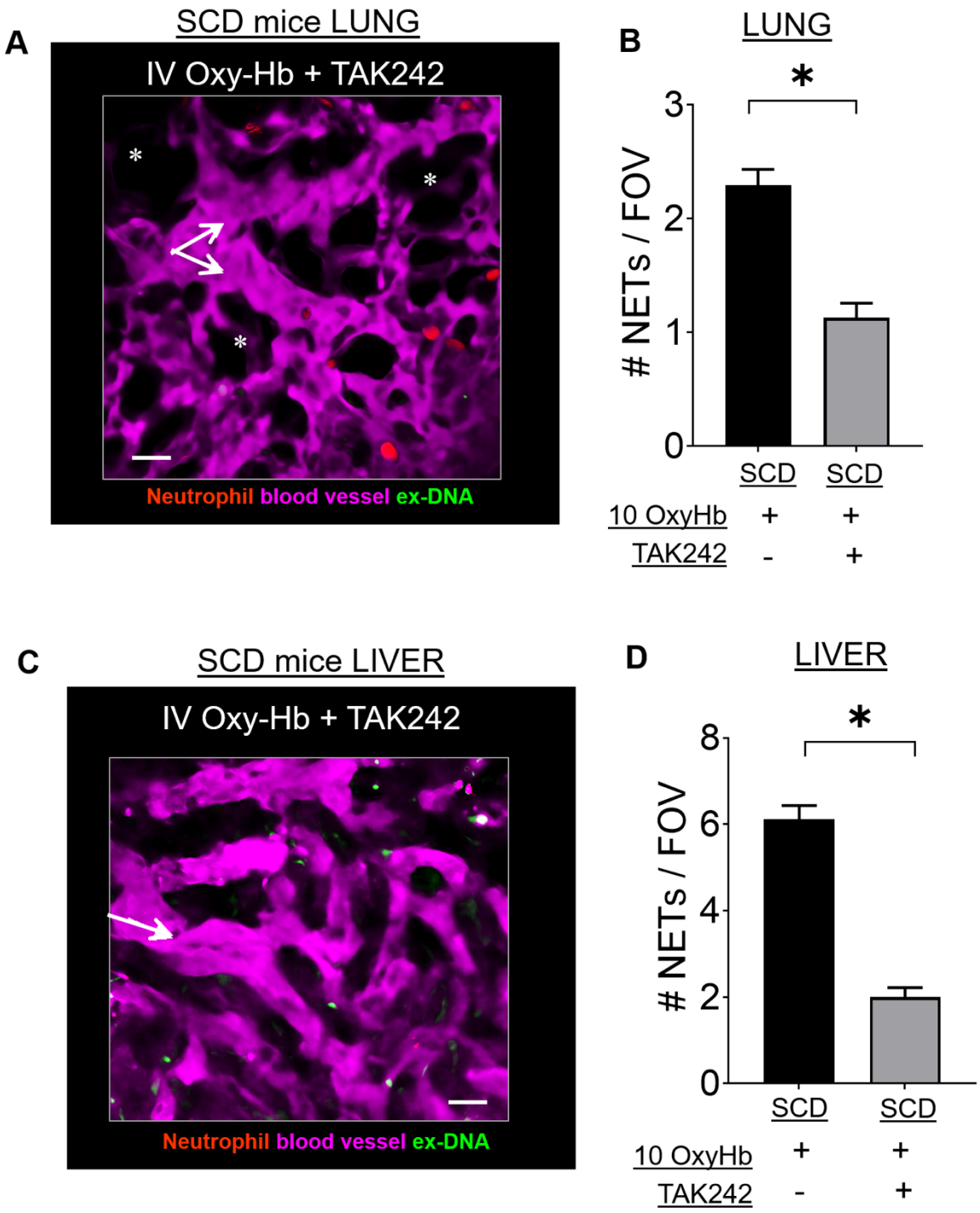

Supplemental Figure 27. TLR4 inhibition attenuates NETs in the lung and liver of SCD mice *in vivo*. SCD mice were IV administered 10 µmole/kg oxy-Hb (10 oxy-Hb) without or with TAK242 (10 mg/kg). Microcirculation, neutrophils and extracellular DNA were labeled *in vivo* by

IV administration of FITC dextran, Pacific Blue-anti-Ly6G Ab and Sytox Orange, respectively, and intravital fluorescence microscopy was used to assess the absence or presence of NETs within the lung (**A-B**) or liver microcirculation (**C-D**). NETs were identified based on colocalization of neutrophil (pseudo-colored red) and extracellular DNA (green) in microcirculation (pseudo-colored purple). Intravital microscopy images were analyzed to estimate the number of NETs per Field of View (#NETs/FOV). Refer Supplemental Methods for details. **(A)** Representative lung intravital image showing absence of NETs in the lung microcirculation of SCD mice IV administered 10 oxy-Hb with TAK242. Alveoli are marked with asterisks. Diameter of pulmonary arteriole~26 µm. **(B)** #NETs/FOV were significantly less in the lung microcirculation of SCD mice IV administered 10 oxy-Hb + TAK242 (n=3 mice; 39 FOVs) than 10 oxy-Hb alone (n=4 mice; 44 FOVs). **(C)** Representative liver intravital image showing absence of NETs in the liver microcirculation of SCD mice IV administered 10 oxy-Hb with TAK242. **(D)** #NETs/FOV were significantly less in the liver microcirculation of SCD mice IV administered 10 oxy-Hb + TAK242 (n=3 mice; 22 FOVs) than 10 oxy-Hb alone (n=4 mice; 44 FOVs). Data represents Mean ± SE and compared using Students *t*-test. * denotes $p < 0.05$. FOV size~65,536 μm^2. Scale bars 20 µm. Arrow denotes the direction of blood flow.

SUPPLEMENTAL VIDEOS

Video 1: Lung intravital microscopy reveals neutrophils (red) and platelets (green) trafficking down the pulmonary arteriole and into the capillaries, suggestive of the absence of pulmonary vaso-occlusion in a control mouse IV administered 10 μmole/kg oxy-Hb. Pulmonary microcirculation (purple). Arrow-blood flow direction. Scale bar 20 μm. Original acquisition rate.

Video 2: Lung intravital microscopy reveals four large aggregates (white ovals) of neutrophils (red) and platelets (green) blocking pulmonary arteriolar bottle-necks in an SCD mouse IV administered 10 μmole/kg oxy-Hb. Pulmonary microcirculation (purple). Arrow denotes direction of blood flow. Scale bar 20 μm. Original acquisition rate.

Video 3: Lung intravital microscopy reveals neutrophils (red) and platelets (green) trafficking down the pulmonary arteriole and into the capillaries, suggestive of the absence of pulmonary vaso-occlusion in a control mouse IV administered 20 μmole/kg hemin. Pulmonary microcirculation (purple). Arrow-blood flow direction. Scale bar 20 μm. Original acquisition rate.

Video 4: Lung intravital microscopy reveals four large aggregates (white ovals) of neutrophils (red) and platelets (green) blocking pulmonary arteriolar bottle-necks in an SCD mouse IV administered 20 μmole/kg hemin. Pulmonary microcirculation (purple). Arrow denotes direction of blood flow. Scale bar 20 μm. Original acquisition rate.

Video 5: Lung intravital microscopy reveals NETs in the pulmonary arteriole bottle-neck of an SCD mouse IV administered 10 μmole/kg oxy-Hb. Pulmonary microcirculation (purple), neutrophils (blue), extracellular DNA (green), and citrullinated histones (red). Arrow denotes direction of blood flow. Scale bar 20 μm. 1/3x original acquisition rate.

Video 6: Lung intravital microscopy reveals NETs in the pulmonary arteriole bottle-neck of an SCD mouse IV administered 10 μmole/kg oxy-Hb. Pulmonary microcirculation (purple), neutrophils (blue), extracellular DNA (green), and neutrophil elastase (red). Arrow denotes direction of blood flow. Scale bar 20 μm. 1/3x original acquisition rate.

Video 7: Lung intravital microscopy reveals NETs (green and red) inside a large neutrophil-aggregate (blue) occluding the pulmonary arteriole bottle-neck in an SCD mouse IV administered 10 μmole/kg oxy-Hb. Pulmonary microcirculation (purple), neutrophils (blue), extracellular DNA (green), neutrophil elastase (red). Arrow-blood flow direction. Scale bar 20 μm. 1/3x original acquisition rate.

Video 8: Lung intravital microscopy reveals circulating NETs (green) entering the lung microcirculation (purple) *via* the pulmonary arteriole in an SCD mouse IV administered 10 μmole/kg oxy-Hb. Neutrophils (red) and extracellular DNA (green). Arrow denotes direction of blood flow. Scale bar 20 μm. 1/3x original acquisition rate.

Video 9: Lung intravital microscopy reveals circulating NETs (green) entering the lung microcirculation (purple) *via* the pulmonary arteriole in an SCD mouse IV administered 10 μmole/kg oxy-Hb. Neutrophils (red) and extracellular DNA (green). Arrow denotes direction of blood flow. Scale bar 20 μm. 1/3x original acquisition rate.

Video 10: Lung intravital microscopy reveals absence of circulating NETs in the lung microcirculation of a control mouse IV administered 10 μmole/kg oxy-Hb. Pulmonary microcirculation (purple), neutrophils (red), and extracellular DNA (green). Arrow denotes direction of blood flow. Scale bar 20 μm. 1/3x original acquisition rate.

Video 11: Liver intravital microscopy reveals vaso-occlusion (white polygon) and neutrophil-associated NETs (white ovals) in the liver microcirculation of an SCD mouse IV administered 10 μmole/kg oxy-Hb. Microcirculation (purple), neutrophils (red), extracellular DNA (green). Colocalization of DNA with neutrophils appear yellow. Arrow-blood flow direction. Scale bar 20 μm. 1/3x original acquisition rate.

Video 12: Liver intravital microscopy reveals neutrophil-associated NETs (white ovals) in the liver microcirculation of an SCD mouse IV administered 10 μmole/kg oxy-Hb. Microcirculation (purple), neutrophils (red), extracellular DNA (green). Colocalization of DNA with neutrophils appear yellow. Arrow-blood flow direction. Scale bar 20 μm. 1/3x original acquisition rate.

Video 13: Liver intravital microscopy reveals neutrophil-associated NETs (white ovals) in the liver microcirculation of an SCD mouse IV administered 10 μmole/kg oxy-Hb. Microcirculation (purple), neutrophils (red), extracellular DNA (green). Colocalization of DNA with neutrophils appear yellow. Arrow-blood flow direction. Scale bar 20 μm. 1/3x original acquisition rate.

Video 14: Liver intravital microscopy reveals NETs fragments (green) detaching from the neutrophil (red) and disappearing into the liver microcirculation (purple) of an SCD mouse IV administered 10 μmole/kg oxy-Hb. Arrow-blood flow direction. Scale bar 20 μm. 1/3x original acquisition rate.

Video 15: Liver intravital microscopy reveals NETs fragments (green) detaching from the neutrophil (red) and disappearing into the liver microcirculation (purple) of an SCD mouse IV administered 10 μmole/kg oxy-Hb. Arrow-blood flow direction. Scale bar 20 μm. 1/3x original acquisition rate.

Video 16: Intravital microscopy reveals absence of NETs in the kidney microcirculation of an SCD mouse IV administered 10 μmole/kg oxy-Hb. Microcirculation (purple), neutrophils (red), extracellular DNA (green). DNA dye (green) is accumulating in glomerular spaces (dark oval structures). Arrow-blood flow direction. Scale bar 20 μm. 1/3x original acquisition rate.

Video 17: Liver intravital microscopy reveals presence and absence of blood flow in the liver of a wild-type mouse pre- and post-clamping, respectively of the portal vein and hepatic artery. Erythrocytes (dark cells) trafficking through microcirculation (purple) before clamping but appear stationary post-clamping. Scale bar 20 μm. Original acquisition rate.

Video 18: Lung intravital microscopy reveals circulating NETs (green) entering lung microcirculation (purple) *via* the pulmonary arteriole, only pre- but not post-clamping of hepatic artery and portal vein in an SCD mouse IV administered 10 μmole/kg oxy-Hb. Neutrophils (red), extracellular DNA (green). Arrow-blood flow direction. Scale bar 20 μm. 1/3x original acquisition rate.

Video 19: Liver intravital microscopy reveals presence of neutrophil-associated NETs (white ovals) and impaired blood flow in the liver microcirculation (purple) of an SCD mouse IV administered 10 μmole/kg oxy-Hb. Neutrophils (red) and extracellular DNA (green). Arrow-blood flow direction. Scale bar 20 μm. 1/3x original acquisition rate.

Video 20: Liver intravital microscopy reveals only a single small NET (white oval) present in the liver microcirculation (purple) of an SCD mouse IV administered 10 μmole/kg oxy-Hb + GSDMD-NT inhibitor LDC7559. Erythrocytes (dark cells) are flowing unobstructed, suggestive of the improved blood flow. Neutrophils (red), extracellular DNA (green). Arrow-blood flow direction. Scale bar 20 μm. 1/3x original acquisition rate.

Video 21: Lung intravital microscopy reveals five aggregates (white ovals) of neutrophils (red) and platelets (green) blocking pulmonary arteriolar bottle-necks in an SCD mouse IV administered 10 μmole/kg oxy-Hb. Pulmonary microcirculation (purple). Arrow denotes direction of blood flow. Scale bar 20 μm. 1/3x original acquisition rate.

Video 22: Lung intravital microscopy reveals absence of pulmonary vaso-occlusion in an SCD mouse IV administered 10 μmole/kg oxy-Hb + pan-caspase inhibitor Z-VAD-FMK. Pulmonary microcirculation (purple) and neutrophils (red). Arrow denotes blood flow direction. Scale bar 20 μm. 1/3x original acquisition rate.

Video 23: Lung intravital microscopy reveals absence of pulmonary vaso-occlusion in an SCD mouse IV administered 10 μmole/kg oxy-Hb + GSDMD-NT inhibitor LDC7559. Pulmonary microcirculation (purple) and neutrophils (red). Arrow denotes blood flow direction. Scale bar 20 μm. 1/3x original acquisition rate.

Video 24: Lung intravital microscopy reveals absence of pulmonary vaso-occlusion in an SCD mouse IV administered 10 μmole/kg oxy-Hb + GSDMD-NT inhibitor Necrosulfonamide. Pulmonary microcirculation (purple) and neutrophils (red). Arrow denotes blood flow direction. Scale bar 20 μm. 1/3x original acquisition rate.

Video 25: Lung intravital microscopy reveals circulating NETs (green) entering lung microcirculation (purple) *via* the pulmonary arteriole, only pre- but not post-clamping of hepatic artery and portal vein in an SCD mouse IV administered 10 μmole/kg oxy-Hb. Neutrophils (red), extracellular DNA (green). Arrow-blood flow direction. Scale bar 20 μm. 1/3x original acquisition rate.

Video 26: Lung intravital microscopy reveals circulating NETs (green) entering lung microcirculation (purple) *via* the pulmonary arteriole, only pre- but not post-clamping of hepatic artery and portal vein in an SCD mouse IV administered 10 μmole/kg oxy-Hb. Neutrophils (red), extracellular DNA (green). Arrow-blood flow direction. Scale bar 20 μm. 1/3x original acquisition rate.

REFERENCES

1. Sollberger G, Choidas A, Burn GL, et al. Gasdermin D plays a vital role in the generation of neutrophil extracellular traps. *Sci Immunol*. 2018;3(26).

2. Rathkey JK, Zhao J, Liu Z, et al. Chemical disruption of the pyroptotic pore-forming protein gasdermin D inhibits inflammatory cell death and sepsis. *Sci Immunol*. 2018;3(26).

3. Tyrkalska SD, Perez-Oliva AB, Rodriguez-Ruiz L, et al. Inflammasome Regulates Hematopoiesis through Cleavage of the Master Erythroid Transcription Factor GATA1. *Immunity*. 2019;51(1):50-63 e55.

4. Vats R, Tutuncuoglu E, Pradhan-Sundd T, Tejero J, Shaw GD, Sundd P. Tandem P-selectin glycoprotein ligand immunoglobulin prevents lung vaso-occlusion in sickle cell disease mice. *Exp Hematol*. 2020;84:1-6 e1.

5. Wu LC, Sun CW, Ryan TM, Pawlik KM, Ren J, Townes TM. Correction of sickle cell disease by homologous recombination in embryonic stem cells. *Blood*. 2006;108(4):1183-1188.

6. Vats R, Liu S, Zhu J, et al. Impaired bile secretion promotes hepatobiliary injury in Sickle Cell Disease. *Hepatology*. 2020;72(6):2165-2181.

7. Vats R, Brzoska T, Bennewitz MF, et al. Platelet Extracellular Vesicles Drive Inflammasome-IL-1beta-Dependent Lung Injury in Sickle Cell Disease. *Am J Respir Crit Care Med*. 2020;201(1):33-46.

8. Ghosh S, Adisa OA, Chappa P, et al. Extracellular hemin crisis triggers acute chest syndrome in sickle mice. *J Clin Invest*. 2013;123(11):4809-4820.

9. Belcher JD, Chen C, Nguyen J, et al. Heme triggers TLR4 signaling leading to endothelial cell activation and vaso-occlusion in murine sickle cell disease. *Blood*. 2014;123(3):377-390.

10. Bennewitz MF, Tutuncuoglu E, Gudapati S, et al. P-selectin-deficient mice to study pathophysiology of sickle cell disease. *Blood Adv*. 2020;4(2):266-273.

11. Shi J, Zhao Y, Wang K, et al. Cleavage of GSDMD by inflammatory caspases determines pyroptotic cell death. *Nature*. 2015;526(7575):660-665.

12. Bennewitz MF, Jimenez MA, Vats R, et al. Lung vaso-occlusion in sickle cell disease mediated by arteriolar neutrophil-platelet microemboli. *JCI Insight*. 2017;2(1):e89761.

13. Bennewitz MF, Watkins SC, Sundd P. Quantitative intravital two-photon excitation microscopy reveals absence of pulmonary vaso-occlusion in unchallenged Sickle Cell Disease mice. *Intravital*. 2014;3(2):e29748.

14. Hu JJ, Liu X, Xia S, et al. FDA-approved disulfiram inhibits pyroptosis by blocking gasdermin D pore formation. *Nat Immunol*. 2020;21(7):736-745.

15. Brzoska T, Kaminski TW, Bennewitz MF, Sundd P. Live Imaging of the Lung. *Curr Protoc Cytom*. 2020;95(1):e80.

16. Brzoska T, Vats R, Bennewitz MF, et al. Intravascular hemolysis triggers ADP-mediated generation of platelet-rich thrombi in pre-capillary pulmonary arterioles. *JCI-Insight*. 2020;5(14):e139437.

17. Yipp BG, Petri B, Salina D, et al. Infection-induced NETosis is a dynamic process involving neutrophil multitasking in vivo. *Nat Med*. 2012;18(9):1386-1393.

18. Slaba I, Wang J, Kolaczkowska E, McDonald B, Lee WY, Kubes P. Imaging the dynamic platelet-neutrophil response in sterile liver injury and repair in mice. *Hepatology*. 2015;62(5):1593-1605.

19. Kolaczkowska E, Jenne CN, Surewaard BG, et al. Molecular mechanisms of NET formation and degradation revealed by intravital imaging in the liver vasculature. *Nat Commun*. 2015;6:6673.

20. Yipp BG, Kim JH, Lima R, et al. The Lung is a Host Defense Niche for Immediate Neutrophil-Mediated Vascular Protection. *Sci Immunol*. 2017;2(10).

21. Chen G, Zhang D, Fuchs TA, Wagner DD, Frenette PS. Heme-induced neutrophil extracellular traps contribute to the pathogenesis of sickle cell disease. *Blood*. 2014;123(24):3818-3827.

22. Wong CH, Jenne CN, Petri B, Chrobok NL, Kubes P. Nucleation of platelets with blood-borne pathogens on Kupffer cells precedes other innate immunity and contributes to bacterial clearance. *Nat Immunol*. 2013;14(8):785-792.

23. Vats R, Kaminski TW, Ju EM, et al. P-selectin deficiency promotes liver senescence in sickle cell disease mice. *Blood*. 2021;137(19):2676-2680.

24. Pradhan-Sundd T, Vats R, Russell JO, et al. Dysregulated Bile Transporters and Impaired Tight Junctions During Chronic Liver Injury in Mice. *Gastroenterology*. 2018;155(4):1218-1232 e1224.

25. Pradhan-Sundd T, Zhou L, Vats R, et al. Dual catenin loss in murine liver causes tight junctional deregulation and progressive intrahepatic cholestasis. *Hepatology*. 2018;67(6):2320-2337.

26. Swamydas M, Luo Y, Dorf ME, Lionakis MS. Isolation of Mouse Neutrophils. *Curr Protoc Immunol*. 2015;110:3 20 21-23 20 15.

27. Sundd P, Gutierrez E, Pospieszalska MK, Zhang H, Groisman A, Ley K. Quantitative dynamic footprinting microscopy reveals mechanisms of neutrophil rolling. *Nat Methods*. 2010;7(10):821-824.

28. Sundd P, Gutierrez E, Koltsova EK, et al. 'Slings' enable neutrophil rolling at high shear. *Nature*. 2012;488(7411):399-403.

29. Oh H, Siano B, Diamond S. Neutrophil isolation protocol. *J Vis Exp*. 2008(17).

30. Jimenez MA, Tutuncuoglu E, Barge S, Novelli EM, Sundd P. Quantitative microfluidic fluorescence microscopy to study vaso-occlusion in sickle cell disease. *Haematologica*. 2015;100(10):e390-393.

31. Zhang X, Ding L, Sandford AJ. Selection of reference genes for gene expression studies in human neutrophils by real-time PCR. *BMC Mol Biol*. 2005;6:4.

32. Group PTC, Calabrese C, Davidson NR, et al. Genomic basis for RNA alterations in cancer. *Nature*. 2020;578(7793):129-136.